A PHASE CORRECTION TECHNIQUE BASED ON SPATIAL MOVEMENTS OF ANTENNAS IN REAL-TIME (S.M.A.R.T.) FOR DESIGNING SELF-ADAPTING CONFORMAL ARRAY ANTENNAS

A Dissertation
Submitted to the Graduate Faculty
of the
North Dakota State University
of Agriculture and Applied Science

By

Sayan Roy

In Partial Fulfillment of the Requirements
for the Degree of
DOCTOR OF PHILOSOPHY

Major Department:
Electrical and Computer Engineering

September 2017

Fargo, North Dakota

NORTH DAKOTA STATE UNIVERSITY

Graduate School

Title

A PHASE CORRECTION TECHNIQUE BASED ON SPATIAL MOVEMENTS OF ANTENNAS IN REAL-TIME (S.M.A.R.T.) FOR DESIGNING SELF-ADAPTING CONFORMAL ARRAY ANTENNAS

By

Sayan Roy

The supervisory committee certifies that this dissertation complies with North Dakota State University's regulations and meets the accepted standards for the degree of

DOCTOR OF PHILOSOPHY

SUPERVISORY COMMITTEE:

Dr. Benjamin D. Braaten
Chair

Dr. David Rogers

Dr. Daniel Ewert

Dr. Alan Denton

Approved:

15th Sep, 2017
Date

Dr. Benjamin D. Braaten
Department Chair

ABSTRACT

This research presents a real-time adaptive phase correction technique for flexible phased array antennas on conformal surfaces of variable shapes. Previously reported pattern correctional methods for flexible phased array antennas require prior knowledge on the possible non-planar shapes in which the array may adapt for conformal applications. For the first time, this initial requirement of shape curvature knowledge is no longer needed and the instantaneous information on the relative location of array elements is used here for developing a geometrical model based on a set of Bézier curves. Specifically, by using an array of inclinometer sensors and an adaptive phase-correctional algorithm, it has been shown that the proposed geometrical model can successfully predict different conformal orientations of a 1–by–4 antenna array in real-time without the requirement of knowing the shape-changing characteristics of the surface the array is attached upon. Moreover, the phase correction technique is validated by determining the field patterns and broadside gain of the 1–by–4 antenna array on four different conformal surfaces with multiple points of curvatures. Throughout this work, measurements are shown to agree with the analytical solutions and full-wave simulations.

ACKNOWLEDGEMENTS

First, I would like to thank my advisor, Dr. Benjamin D. Braaten, for his continuous support, patience, and guidance in completing this research. He always supported me by providing intriguing fundamental thoughts for this research. Without his guidance, I would have never been able to complete this work.

I want to extend my gratitude and thankfulness to my committee members, Dr. David A. Rogers, Dr. Daniel L. Ewert and Dr. Alan R. Denton, for their continuous encouragement and support. They have taught me many things and helped me in overcoming any difficulties I had along the way in this research.

I acknowledge the Graduate School of the North Dakota State University for providing financial support for this project through the 2014 Doctoral Dissertation Fellowship Award.

I acknowledge the IEEE Antennas and Propagation Society for providing me the travel support for attending and presenting proceeding related to this topic in the 2015 IEEE AP-S Symposium on Antennas and Propagation at Vancouver, British Columbia, Canada.

I would especially like to thank Dr. Neil F. Chamberlain with the NASA Jet Propulsion Laboratory (JPL), California, Dr. Sayeed J. Sajal with the Minot State University, North Dakota and Dr. M. Bilal Qureshi with the COMSATS Institute of Information Technology, Pakistan for their collaboration and input on various aspects of this research.

I am grateful to the IEEE AP/MTT Chapter in Kolkata, India for inviting me to a talk session and thus providing me a great platform to discuss and share my research ideas and experiences.

Finally, I would like to thank my family. I am indebted to my parents and my wife for their continuous caring and motivation throughout my graduate career.

DEDICATION

This thesis is dedicated to

my mother, *Sampa Roy*, and my father, *Subhrangshu Kumar Roy*, for their constant motivation, support and understanding to the choices I made so far in my life,

and

my beautiful wife, *Swati*, for her endless love, caring and patience to deal with me *24*$\times$*7*.

PREFACE

The fields of antennas and wave propagation have drawn the attention of researchers for the last thirty years resulting in many inventions of new types of antennas with superior performance and versatile features. The conformal antenna is one of these new types of antennas. A conformal antenna is described as an antenna that conforms to a prescribed shape. The shape can be some part of an airplane, a spacesuit, a high-speed train or other types of physical entities. Usually, a conformal antenna is cylindrical, spherical, or some other shape, with the radiating elements mounted on or integrated into the smoothly curved surface.

TABLE OF CONTENTS

LIST OF TABLES

LIST OF FIGURES

1. INTRODUCTION

"*Daher ist die Aufgabe nicht sowohl zu sehen was noch keiner gesehen hat, als bei Dem was Jeder sieht, zu denken was noch Keiner gedacht hat.*"
Translated: "*Therefore the problem is not so much, to see what nobody has yet seen, but rather to think concerning that which everybody sees, what nobody has yet thought*."

— **Arthur Schopenhauer**, *"Parerga und Paralipomena"*.

1.1. History

Electromagnetism is a versatile and rich branch of physics. Study on electromagnetism deals with exploring the theoretical background and practical applications of movement of photons and interactions of electric and magnetic fields in environments of different properties. The cause and effect of electromagnetism are due to the presence and involvements of electromagnetic forces with different kinds of potential gradient or fields in various mediums. The electromagnetic force is one of the four fundamental forces, viz. Gravitational Force, Weak Nuclear Force, Strong Nuclear Force, and Electromagnetic Force. From classical electrodynamics to quantum mechanics, the consequences of electromagnetism are endless.

Surprisingly, the concept of the electromagnetic phenomenon was very rudiment until the beginning of 19^{th} century. However, in the next 100 years, many great scientists and physicists would contribute their lifetime work to discover and formulate the mathematical and experimental theories of electromagnetics which would change the perception of communication in the world forever. Around 1820, an accidental observation of the deflection of a compass needle by a nearby current carrying conductor led Ørsted, a Danish physicist and chemist, to conclude that current through the conductor generated a magnetic field [1]. After a decade, Ampère, a French physicist and mathematician, formulated the analytical relationship that describes how a magnetic force generates around a current-carrying conductor [2]. Over the next thirty years, the great experimental English scientist Faraday invented many useful ways, such as the very first examples of motor (1821) and inductor (1831), by using the interactions of varying electric and magnetic fields in electrical circuits [3]. Based on the observations made by Faraday, the breakthrough on the research of theoretical electromagnetics happened in 1873 when a legendary Scottish mathematical physicist

named Maxwell presented a set of twenty partial differential equations with twenty variables on the interactions of electric and magnetic fields [4]- [5]. In his textbook, *A Treatise on Electricity and Magnetism*, Maxwell presented a unified form of oscillating electric and magnetic fields to mathematically describe how energy can travel over different mediums in the form of electromagnetic waves. Later in 1881, Heaviside, a self-taught English engineer, simplified and combined Maxwell's twenty equations to only four partial differential equations which are well-known today as Maxwell's equations [6]. Then, it took just five years by Hertz, a German physicist, to prove the existence of electromagnetic waves in free-space by incorporating Maxwell's equations into electrical circuits. In 1886, Hertz built the first wireless communication system in his laboratory by using a set of conductors shaped of cylindrical rods and circular loops which were a set of primitive dipole antennas and loop antennas, respectively [7]. After a decade, Bose, an eminent scientist from India (then British India), generated radio frequency of millimeter range wavelength by developing microwave transmitter and receiver using millimeter waveguides, horn antennas, and most importantly a primal semiconductor junction as a microwave detector. In 1896, he successfully demonstrated the phenomenon of wireless communication within short range [8]. During this same time, Tesla, a renowned Serbian-American inventor, developed few novel techniques to transfer electrical signal wirelessly over long distances [9]. Between 1901-1902, an Italian inventor named Marconi successfully demonstrated transatlantic wireless communication for the first time [10]. In 1905, the invention of the phased array antenna by a German physicist named Braun by controlling the direction of radio signals using selective signal feeding at precise time intervals to the elements of an antenna array (he used three monopoles) [11] led Braun and Marconi to share the Nobel Prize in Physics in 1909. For the next few decades, research investments in wireless communications had surged worldwide due to the interests of various countries during the two world wars. Significant developments in the research of phased array antennas have been since continued due to its ability to steer the course of maximum radiation of transmitted or received power (beam steering of main lobe) to any desired direction by changing the signal amplitude and phase related to the individual elements in the array. The resulting field pattern of an array antenna depends on five array parameters [12]:

1. the geometrical configuration of the overall array
2. the relative displacement between the elements

3. the excitation amplitude of the individual elements

4. the excitation phase of the individual elements

5. the relative pattern of the individual elements.

1.2. Conformal Antenna

A conformal antenna is a speacial kind of antenna that conforms to a precribed shape. The IEEE Standard Definition of Terms for Antennas (IEEE Std 145-1993) gives the following definition:

2.74 conformal antenna [conformal array]. An antenna [an array] that conforms to a surface whose shape is determined by considerations other than electromagnetic; for example, aerodynamic or hydrodynamic [13].

1.3. Motivation for Work

Lately, the availability of certain emerging technologies such as flexible RF circuits using additive manufacturing [14]- [16] and electro-textiles [17] have fostered the research and development of conformal antennas on mechanically agile and wearable surfaces. On the other hand, the versatility of conformal antennas on non-planar surfaces has generated significant attention in the automotive, aviation, and space industries [18], unlike conventional planar antennas with very limited or no mechanical flexibility. The initial investigation of flexible and adaptive antennas dates back to 1973 [19], and recent studies [20]- [24] on self-adapting and flexible arrays have laid the foundations for modern day conformal antenna arrays. Although most of them have shown interest in placing the antenna on a conformal surface, but none of them considered the performance of the antenna to be optimum through a correction method, which will be self-adaptable for real-time operation. Additionally, these previous works require some initial knowledge of the conformal surface (i.e., wedge-, cylindrical- or spherical- shaped).

2. PATTERN CORRECTION TECHNIQUE OF PLANAR CONFORMAL ARRAY ANTENNAS USING VIRTUAL PROJECTION METHOD

"*It is even possible to create an antenna array that can adapt its performance to suit its environment. The price paid for these attractive features is increased complexity and cost.*"

— **Randy Haupt**, *"Antenna Arrays: A Computational Approach"*.

2.1. Introduction

This chapter presents the details involved with conformal antenna array. In general, conformality means preserving the correct angles within small areas, though distorting distances. Specifically for a conformal antenna, the antenna system is deployed to work on a non-planar surface in such a way that the performance of the antenna remains unchanged with respect to the performance of the antenna that has been placed on a flat surface. However, in this chapter, only two different kinds of planar yet non-flat orientations of conformal antenna array have been presented for simplicity. Particularly, the background and scanning techniques for correcting the field pattern of a planar conformal antenna array will be discussed in this chapter for a better understanding of the theory.

2.2. Concept of Antenna Array

An antenna array is a set of N antenna elements. Practically, the value of N has a range from 2 to several thousands, as in the AN/FPS-85 Phased Array Radar Facility operated by U. S. Air Force [25]. The reason why the array is more popular than its equivalent single-element prototype is that the array introduces the ability to scan not only the frequency band but also the coverage area without increase in size of the total system. Based on different types of spacial distributions of the elements and application of signal processing units in the array, an array antenna can offer superior performance to an individual element in terms of bandwidth and directivity [12].

The fields radiated from a linear array are a superposition of the fields radiated by each element in the presence of the other elements. Each element has an excitation parameter, which is current for a dipole, voltage for a slot and mode-voltage for a multiple-mode element. Obviously, the

individual excitation of each element will be a complex number, with distinct amplitude and phase. This discrete distribution is called an aperture distribution where the array is the aperture.

2.3. Phased Array Antenna

One popular way to achieve electronic scanning in an antenna arrays is to feed the array elements by means of phase shifters in a way that the phase variations along the array follow an arithmetical progression whose common difference is the phase shift between two adjacent elements. Let us consider an array of eight ($N = 1, 2, 3, ..., 8$) identical antennas, with an equal inter-element spacing of d, radiating to the broadside direction ($\theta = 0°$), as shown in Fig. 2.1. When all the elements of the array are connected by a feed netwrok and when each of them are excited by a progressive phase difference ($\Delta\phi$), the waves transmitted by individual element of the array generate identical wavefronts at different times. Hence, a resultant equiphase plane appears at a different angle other than the broadside ($\theta \neq 0°$). Thus the array generates a plane wave at a certain angle (θ) whose direction depends on the controlled phase interval ($\Delta\phi \propto d \sin\theta$) [26].

2.4. Functional Blocks of Phased Array Antenna

Any phased array antenna in general, apart from the array elements, consists of two functional blocks known as the feed network and the phase scanning circuitry. Each of these blocks plays very important roles for the correct functionality of the array and are described here in detail.

2.4.1. Feed Network

A feed network distributes energy to the elements of the array by means of phase shifters according to a desired amplitude function. A corporate binary feed, as shown in Fig. 2.1 is common in arrays of dipoles, open-end guides and microstrip patch antennas. Such feed circuits are commonly binary but can be modified to design 3-way or 5-way dividers, depending upon the number of array elements. The critical component in the corporate feed is the power divider that can be realized by bifurcated T waveguide or coaxial T junctions [27]. One challenge in designing of this type of feed network is that each of the elements is required to be impedance matched and isolated or the reflected signal from any other element may result an unwanted parasitic radiation pattern that will be superimposed on the required pattern. This condition plays an important role in the design of feed networks, where it is often necessary to use a directional couplar or a matched transmission line.

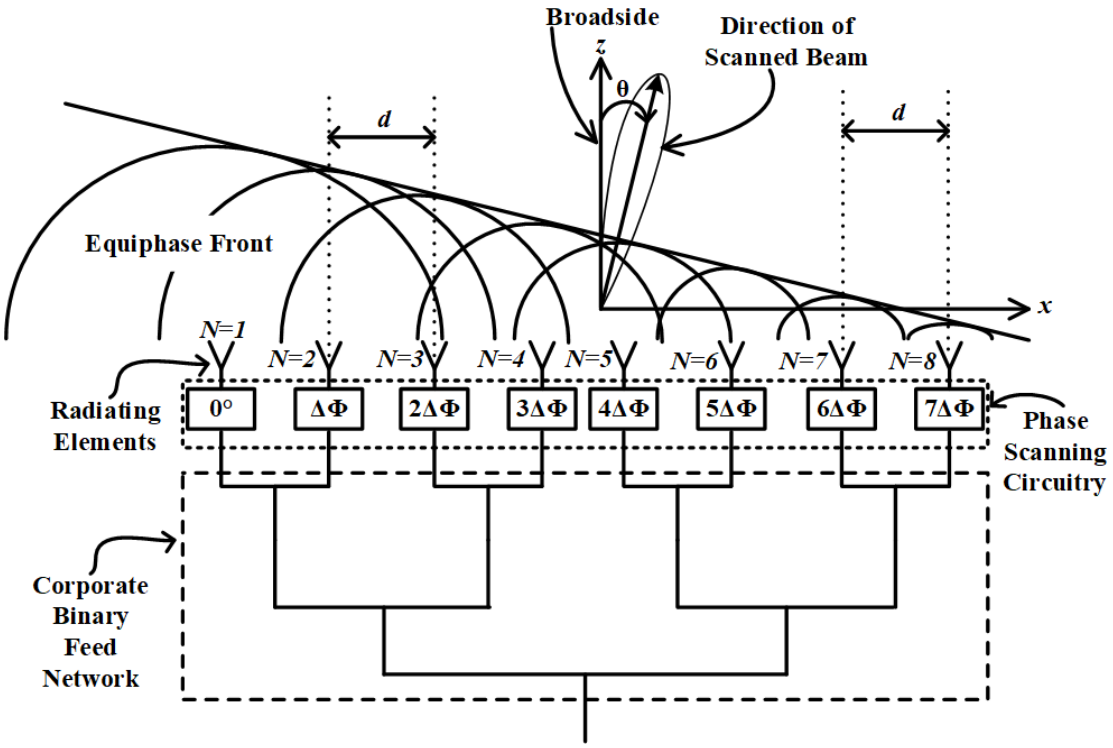

Figure 2.1. A phased array antenna with corporate feed network and phase scanning circuitry.

2.4.2. Phase Scanning Circuitry

One primary goal of developing phased-array antennas is to achieve beam steering electronically and thus to eliminate the mechanical movement of an antenna system. Electronic beam steering in an array can be realized by time delay scanning, frequency scanning or phase scanning techniques. However, ease of implementation, cheaper digital control circuits, fast response time and high sensitivity make the phase scanning method the most popular. For proper functionality, a clever choice for a phase shifter is a switched line or ferrite phase shifter with analog or digital control. A good choice for the placement of phase shifters along the feed line is also a very important factor. The orientation may be in series or in parallel, as shown in Fig. 2.2. Although the series phasers have the advantage of sharing equal power, the disadvantage is the phase compensation circuit because the basic interelement phase shift must be multiplied by the number of elements and small amount of attenuation or even a little impedance mismatch of the phasers may add up

along the feed line. On the contrary, for a parallel combination, although each phase shifter does not share the same power, the major advantage is all phasers are independent of each other and thus modeling of the control circuit becomes simpler. The mathematical approach to the phase compensation calculation will be discussed in the next section.

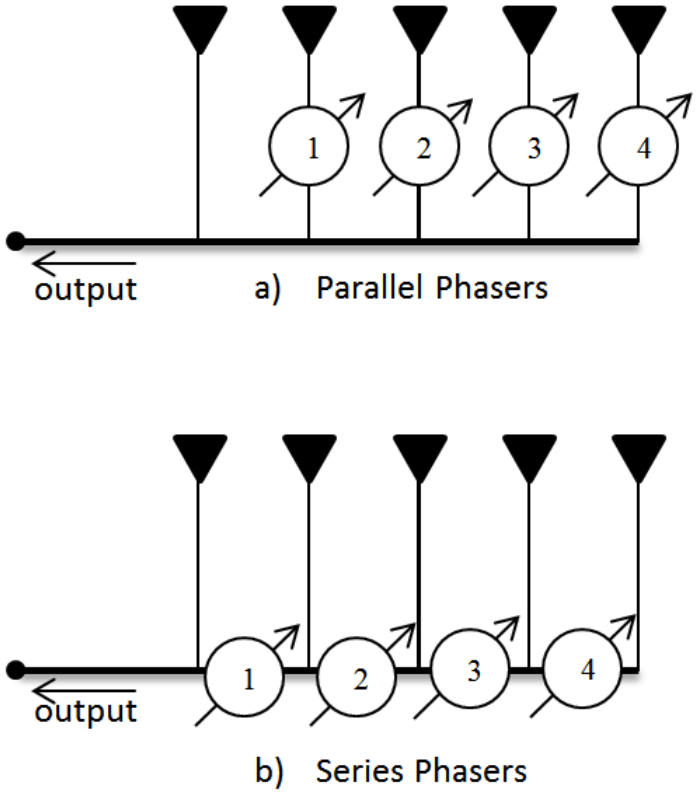

Figure 2.2. Parallel and series feeds.

2.5. Defining Coordinate System

For notation purposes, henceforth it will be assumed that any linear planar array will be lying on the $x-y$ plane with the z-axis pointing broadside to the array unless otherwise mentioned, as shown in Fig. 2.3. One objective of this project is to build an array system for a receiver: therefore, any antenna system will be considered as a receiver module with respect to a point source acting as a transmitter, as shown in Fig. 2.4. The rectangular coordinate system has been used throughout

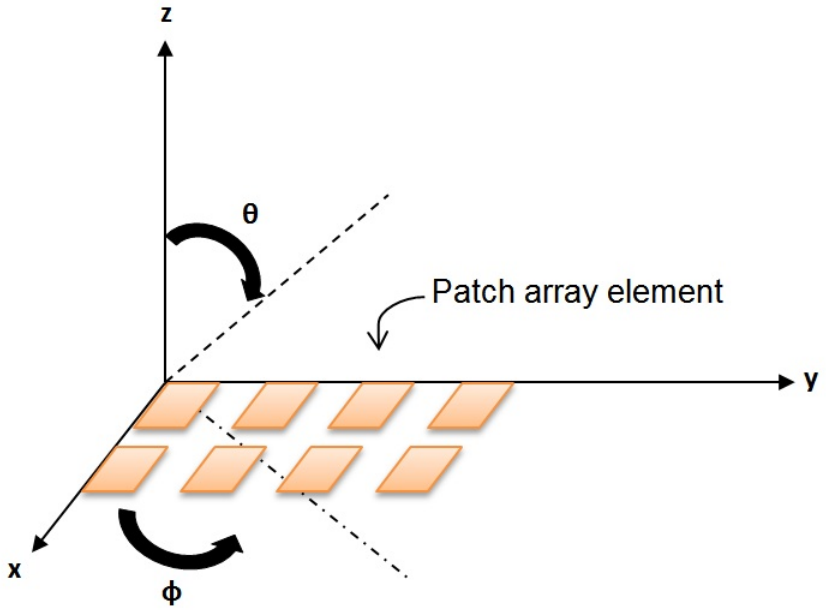

Figure 2.3. Distribution of elements of a 2×4 patch antenna array on the $x-y$ plane.

the discussion, with proper notation. To define the angular separation of the array element from an axis, two parameters have been defined, denoted as the elevation angle or scan angle (θ) and the azimuthal angle (ϕ). The scan angle is defined as the angular separation of the elements from the broadside direction or specifically, the z axis. The azimuthal angle has been defined as the angle between the elements and x axis, as shown in Fig. 2.3. Now considering the Cartesian coordinate system, a new parameter has been defined here,

$$\Psi_n = k(x_n u + y_n v) \tag{2.1}$$

where

$$k = \frac{2\pi}{\lambda}. \tag{2.2}$$

(x_n, y_n) is the location of the n^{th} element in the $x-y$ plane, k is the wave number and

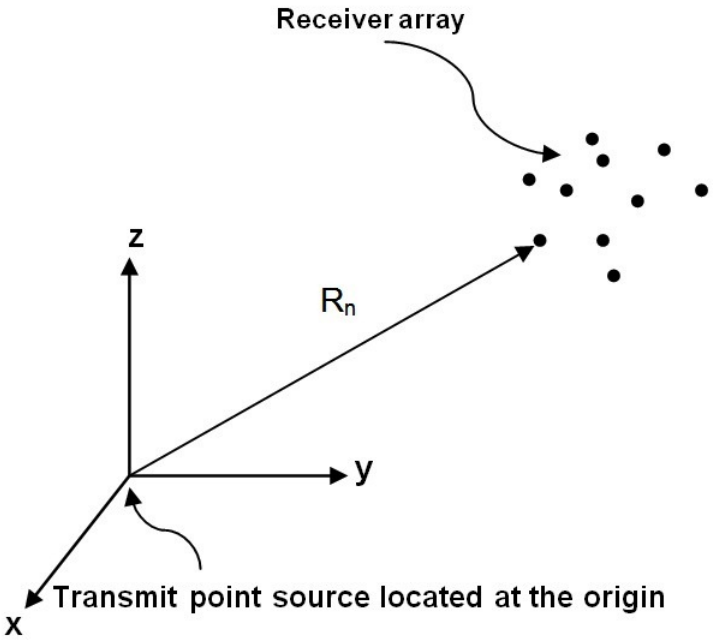

Figure 2.4. Array system with a point source transmitter.

$$u = \sin\theta\cos\phi, \tag{2.3}$$

$$v = \sin\theta\sin\phi. \tag{2.4}$$

2.6. Controlling Parameters of an Array Antenna System

Two important properties of any individual antenna are return loss and radiation pattern. Return loss is the measurement of impedance mismatch along the path of propagation of the signal. Often termed as (S_{11}), this parameter determines the reflection coefficient (Γ) of the system. The radiation pattern or the field pattern describes the angular dependency of the strength of the radiowaves received by the antenna, usually expressed in dB (and sometimes in dBi to emphasize a comparison with the field pattern of an isotropic radiator). But when multiple antennas are used to form an array, as shown in Fig. 2.5, there are several factors that determine the behavior of the antenna array [12]. These are discussed below.

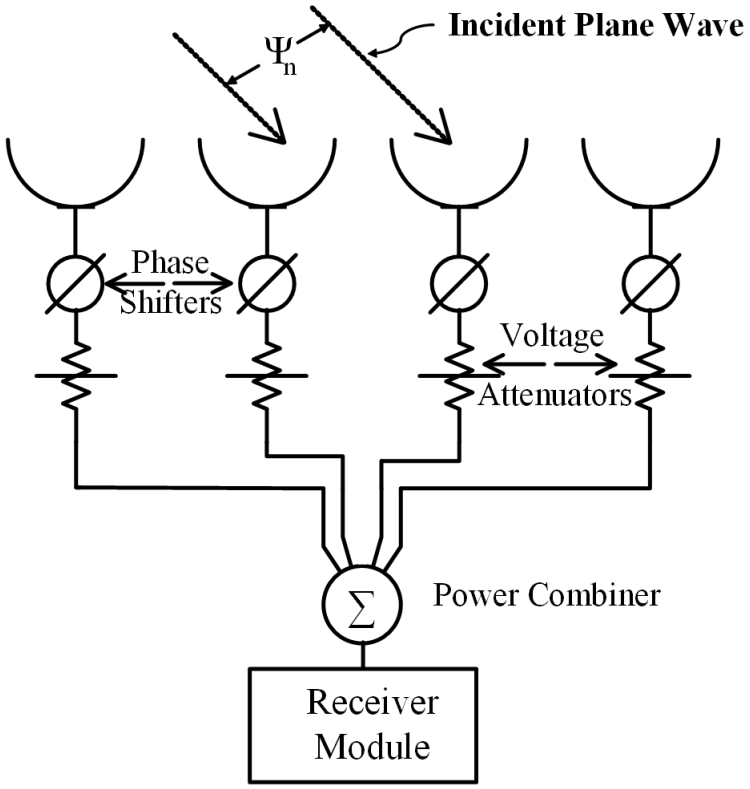

Figure 2.5. A typical linear array system with variable phase shifter (shown as circular blocks) and attenuator (shown as variable resistor block) segments designed to be operated as a receiver module.

2.6.1. Geometrical Orientation of the Overall Array

The geometrical orientation of the array may be linear, planar, circular, spherical etc. in nature. When the array elements lie along a straight line, it is a linear array and when the elements are located on a plane, it is a planar array. Depending upon the spatial distribution of the array elements, a planar array may be designed as a circular or rectangular array. However, for each of the cases, the effective field distribution and mutual coupling will be different from one another.

2.6.2. Relative Separation between the Elements

The relative spacings between the elements of the array determines the position of the peak and the null of the field pattern, and hence, careful choices need to be made during the design of an array.

2.6.3. Excitation Amplitude of the Individual Element

Amplitudes of the current on the elements of an array can be varied to shape the beam and control the level of the sidelobes of the array. This phenomenon is known as amplitude tapering and the arrays of these types are termed as *non-uniformly excited arrays* [28].

2.6.4. Excitation Phase of the Individual Element

The relative phases of the currents on each individual element of an array can be controlled to reinforce the field pattern of the array in a particular direction. These types of arrays are known as phased array antennas.

2.6.5. Relative Pattern of the Individual Element

The overall response of the array is the superposition (sum) of all individual elements of the arrays excited separately and thus can be mathematically determined by a Fourier transformation. To avoid complexity in terms of design and calculation, generally arrays are considered to be made of identical elements.

2.7. Array Factor

An important parameter related to the array antenna is the Array Factor (AF) which is unique for each array and depends on various parameters such as the number of elements of the array and their geometrical arrangements, relative magnitude, phase shift and interelement spacing. If $\mathbf{E_s}$ represents the electrical field due to a single element in a linear array and if the AF is the array factor of that array, then the total electrical field, $\mathbf{E_{total}}$, at the far-field of the array can be expressed as [12]:

$$|\mathbf{E_{total}}| = [\mathbf{E_s}][\mathrm{AF}] \tag{2.5}$$

provided all the elements of the array are identical in nature. This concept can be used even if the actual elements are not isotropic sources. Then the total field can be determined by multiplying the array factor of the array made of isotropic sources and the field due to a single isotropic element. This concept is known as pattern multiplication and can be a very powerful tool for practical cases where elements of an array are not isotropic sources [12]. For a system where an isotropic point source is the receiver, the field of the array turns out to be proportional to the weighted sum of the received signal from each element in the array. The far-field radiation pattern is the discrete Fourier transform of the array excitation [12]. The array notation used here is θ as the angle from broadside, θ_0 being the scan angle, d as the element spacing and λ as the corresponding

wavelength. Mathematically [27],

$$|\mathbf{E}(x_f, y_f, z_f)| \propto \sum_{n=1}^{N} w_n \frac{e^{jkR_n}}{R_n} \tag{2.6}$$

where R_n is the distance from the n^{th} array element to the point (x_f, y_f, z_f) in a rectangular coordinate system. The phase of the received signals at the element will be positive as the signal is travelling toward the element. When the array is very far from the point source, then R_n in the denominator of equation (2.6) are approximately the same $\forall n$. Consequently, the resulting field is proportional to the sum of the weighted phase vectors and can be expressed as [27],

$$|\mathbf{E}(x_f, y_f, z_f)| \approx \sum_{n=1}^{N} w_n e^{jkR_n}. \tag{2.7}$$

Generally, arrays are either planar or linear. To make calculations easy, henceforth it will be assumed that the array elements lie along the x, y or z axes under normal conditions. The phase reference or the point of zero phase can be regarded to be any element of the array. However, the origin of the coordinate system should be considered to be placed at the phase center to reduce calculation complexity. An incident plane wave arrives at all of the elements at the same time when the incedent field is normal or broadside to the array. When the plane wave is off-normal, then the plane arrives at each element at a different time. Thus, the phase differences between the signals received by the elements are accounted for an appropriate phase delay before summing the signals to get the array output [27]. For the calculation of phase delay and array factor, a spherical coordinate system has been used here. Conversion from a spherical coordinate system to its equivalent cartesian coordinate system and vice-versa have been given in equation (2.8).

Let us consider that an element is lying at (R, θ, ϕ) in a spherical coordinate system as shown in Fig. 2.6. Now for any incident wave vector located on the $x - y$ plane, the phase will be a function of ϕ and for any incident wave vector located on the $y - z$ plane, the phase will be a function

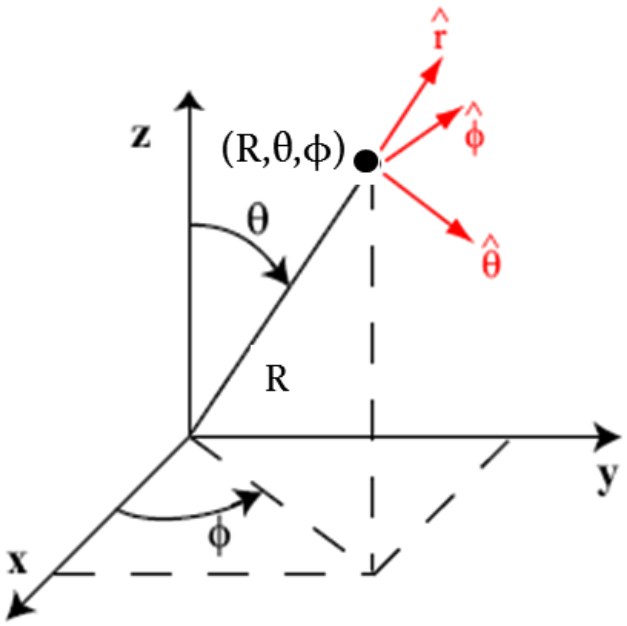

Figure 2.6. Spherical coordinate system.

of θ where

$$\left.\begin{aligned} x &= R\sin\theta\cos\phi, \\ y &= R\sin\theta\sin\phi, \\ z &= R\cos\theta, \\ R &= \sqrt{x^2+y^2+z^2}, \\ \phi &= \tan^{-1}\left(\frac{y}{x}\right), \\ \theta &= \cos^{-1}\left(\frac{z}{\sqrt{x^2+y^2+z^2}}\right). \end{aligned}\right\} \tag{2.8}$$

and

If w_n is the complex weight factor for element n, then the array factor AF due to isotropic point sources is a weighted sum of the signals received by the elements and can be expressed as:

$$AF = \sum_{n=1}^{N} w_n e^{j\Psi_n} \tag{2.9}$$

where

$$w_n = a_n e^{j\delta n}, \tag{2.10}$$

(x_n, y_n, z_n) is the location of the n^{th} element,

(θ, ϕ) is the direction in space

and

$$\Psi_n = \begin{cases} kx_n u = kx_n \cos\phi \; or \; kx_n \sin\theta, & \text{along x axis;} \\ ky_n u = ky_n \sin\phi \; or \; ky_n \sin\theta, & \text{along y axis;} \\ kz_n \cos\theta, & \text{along z axis.} \end{cases} \tag{2.11}$$

2.8. Phase Steering

By controlling the progressive phase difference between each individual element of an array, the field pattern of the array can be reinforced in certain directions to form a scanning array. In Fig. 2.7, the change of direction of maximum radiation of an array has been shown graphically. Let us assume, the maximum radiation of the array is required to be in the direction $u = u_s$. Now, the direction of maximum radiation refers to the peak of the main beam of the field pattern of the array. But, at the peak of the main beam, the array factor has the maximum value of:

$$AF_{max} = \sum_{n=1}^{N} w_n. \tag{2.12}$$

Therefore, without moving the antenna physically this condition can be achieved by adding a constant phase shift δ_n to the parameter Ψ_n. Now mathematically,

$$\Psi_n = kx_n u + \delta_n. \tag{2.13}$$

But according to equation (2.12), $\Psi_n = 0^\circ$ for the desired steering direction, earlier defined by $u = u_s$.Therefore,

$$\Psi_n = (kx_n u + \delta_n)|_{u=u_s}.$$

$$\Rightarrow \delta_n = -kx_n u_s. \tag{2.14}$$

This is the basic principle of electronic scanning for phased array operation. Practically, continuous scanning can be realized using commercially available phase shifters which are available as either

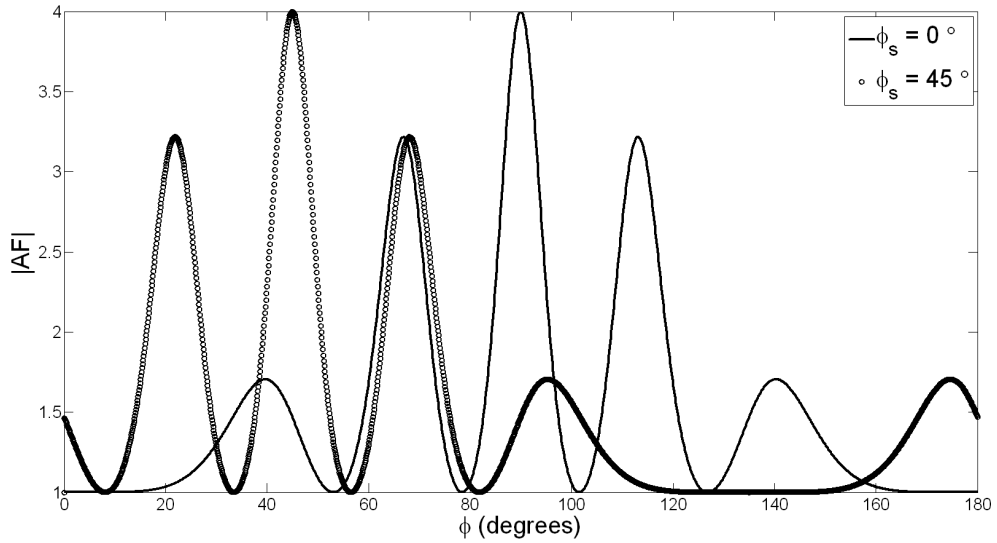

Figure 2.7. Direction of maximum radiation of a 1×4 planar array steered 45° toward the left by incorporating a progressive phase difference along the array elements.

ferrite-based or diode phase shifters. However, to achieve a fixed phase difference, one can also apply the theory of path delay by introducing equivalent length of signal trace on the path of signal propagation to individual elements in the array.

For a complete discussion on this issue, let us consider a phase steering example of a phased array system consisting of 4 elements along x-axis with element spacing of 0.5λ. Now steering the beam to 45°, as shown in Fig. 2.7, requires a phase at the n^{th} element of value δ_n where δ_n can be computed using equation (2.14) and can be expressed as,

$$\delta_n = -cos(45^\circ) \times \frac{2\pi}{\lambda} \times 0.5\lambda \times (n-1).$$

$$\Rightarrow \delta_n = -0.707\pi(n-1) \quad \text{radians.} \tag{2.15}$$

The above mathematical model of the theory of phase steering can thus be validated for any array antenna system. This validation, in particular, leads to the motivation of designing a conformal array antenna. In the case of a conformal array antenna, the surface of the substrate can be changed between different planar orientations during the time of operation. Now, when the surface remains flat, the system behaves normally. However, as the surface changes from a flat orientation, not

only the distances between the elements of the array change, but also the direction of maximum radiation differs for each individual element. These changes lead to an overall distorted field pattern of the array. By using the concept of phase steering, the direction of maximum radiation of the array can then be controlled by introducing phase correction. Moreover equation (2.14) suggests that δ_n also depends on the geometrical placement of the n^{th} element, given by x_n from the origin in the Cartesian coordinate system.

2.9. Realization of Phased Array Antenna

Let us consider a 1x4 linear microstrip patch antenna array in the $x-y$ plane, as shown in Fig. 2.8. The array, as shown, consists of four identical microstrip rectangular patches. Therefore if the amplitude and phase of excitation current on each individual element of the array are the same, there will be no change in the behavior of the array. An angle ϕ_s has been defined here as the angle between the direction of maximum radiation and the x-axis. It is assumed that the direction of maximum radiation is broadside to the array. This angle ϕ_s is then equal to $\pi/2$ when the array elements are considered to be placed on the $x-y$ plane.

The main objective of this work is to rescue the radiation pattern of the conformal array during its nonplanar activity. Since broadside radiation is desired, it will be expected that the effective driving current on each individual element has to be kept equal in terms of amplitude and phase. Then only the fields radiated from each element will arrive in the same manner to any plane along the broadside direction. The two dimensional orientation of the array in both planar and nonplanar stages have been shown in Fig. 2.9. A circular nonplanar orientation can also be designed which will be discussed later. First we will consider correction of phase of a conformal antenna on a wedge shaped surface as shown in Fig. 2.9. The grey dotted line in Fig. 2.9 defines the position of the array in a planar flat orientation and the solid line defines the position of the array after bending into a planar non-flat orientation. The angle ϕ_s, described earlier is shown here. A new parameter θ_w has been introduced in this section to define the angular separation between the two planes of the array after bending. In practice, this situation can be realized by placing the array on a wedge with angle θ_w made up of a non-conducting material such as wood or Styrofoam. The antenna elements situated on the positive $x-$axis are denoted as A_{+n} and the elements situated on the negative $x-$axis are denoted as A_{-n} where n is the number of elements of the array with respect to the center of the array, located at the origin. The field from each element $A_{\pm n}$ has been denoted as $\mathbf{E}_{\pm n}$. If (x_n, z_n) is the location of the n^{th} element of the linear conformal array in Fig. 2.9, then, for a non-flat

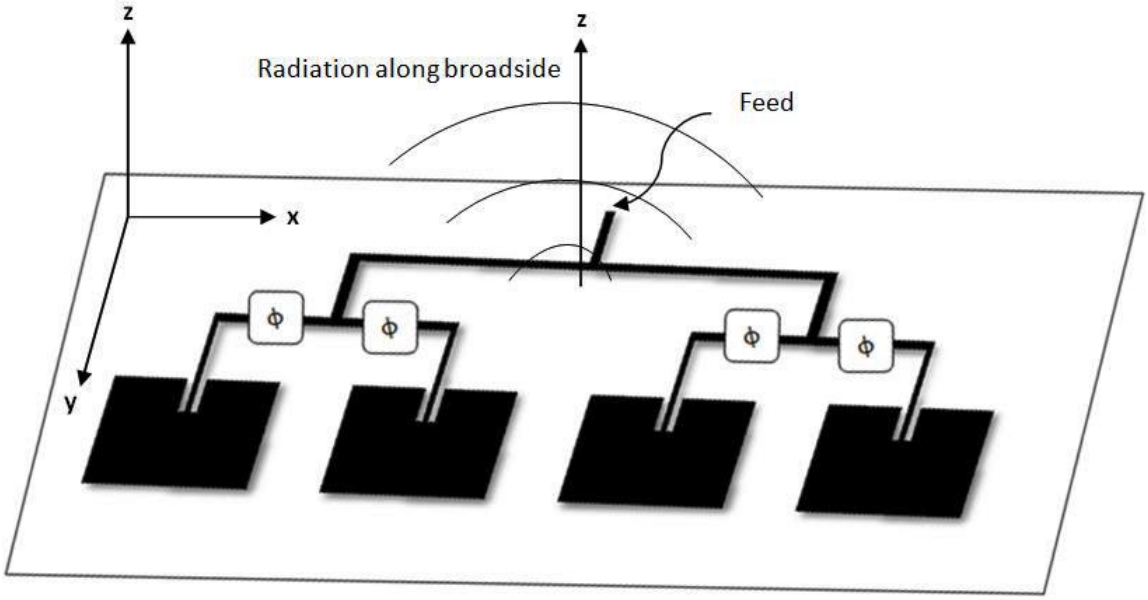

Figure 2.8. 1x4 Microstrip patch antenna array.

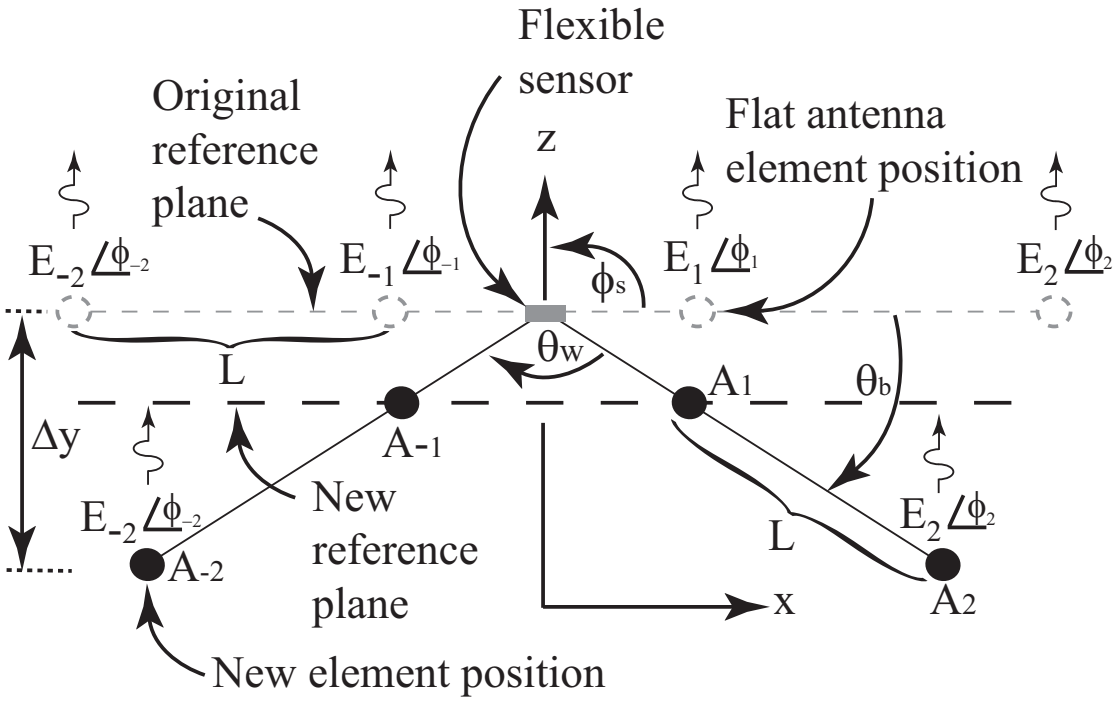

Figure 2.9. Phase compensation of a linear array on a single curved surface shaped as a wedge.

orientation of the array, an $x-$ and $z-$translation will be incurred from the original flat position for each array element. Now, when the fields from $A_{\pm 2}$ arrive at the new reference plane, as shown in Fig. 2.9., they will lag the radiated fields from element $A_{\pm 1}$ due to the observation of negative phase along the propagation of the free space wave. Therefore the phases of current at $A_{\pm 2}$ should be positive enough to compensate for the phase delay introduced by that free space propagation to ensure that the fields arrive at the new reference plane with the same phase for broadside radiation. Clearly, this phase delay depends upon the angle θ_w. The amount of free-space phase introduced by the propagation of the wave from elements $A_{\pm 2}$ to the new reference plane can be computed by using the equation below [29],

$$\delta_n = -k(|x_n| \cos \phi_s + |z_n| \sin \phi_s). \tag{2.16}$$

Now as mentioned earlier, the primary concern of this work is to maintain the radiation pattern in the broadside direction. So it can be inferred that irrespective of any value for θ_w, the value of the scan angle ϕ_s will be considered to be $\pi/2$. This then simplifies equation (2.16) to

$$\delta_n = -k|z_n|. \tag{2.17}$$

Next, the required phase compensation has been calculated using θ_w. Consider the case when the 1×4 array is attached to the conformal surface shown in Fig. 2.9. The phase of the current at each element will be different with respect to each other during receiving a signal from a transmitter at the far-field. This will eventually lead to a distorted radiation pattern of the array. This can be described as follows. Under flat conditions when the array is acting as a planar array, the electric fields radiated from each antenna leave the original reference plane with the same phase to create a broadside radiation pattern. However, when the array is placed on a wedge shaped surface, situated at the origin, the geometrical orientation of the elements changes. As Fig. 2.9 suggests, the position of elements A_{+1} and A_{-1} now belong to a new plane, shown as the black dotted line and the position of elements A_{+2} and A_{-2} belong to another new plane. So now, when any signal from the far-field will be received by the array, the elements of the array will no longer receive the signals coherently. Mathematically, the predefined angle ϕ_s will be changed therefore for the nonplanar application of the array as the array elements will be then excited with signals with different attributes. As shown,

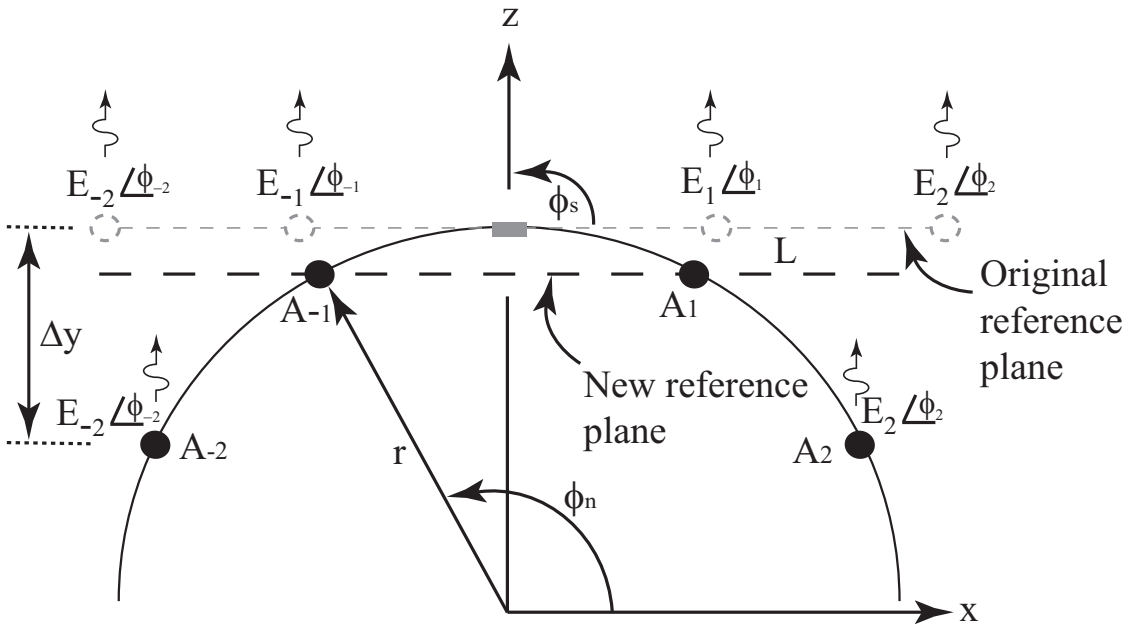

Figure 2.10. Phase compensation of a linear array on a single curved surface shaped as a cylinder.

the signals received by $A_{\pm 2}$ have to travel a path distance more than the signals received by $A_{\pm 1}$ where this path distance is the linear separation between those two planes where the elements $A_{\pm 1}$ and $A_{\pm 2}$ are lying. From Fig. 2.9, this path distance can be calculated in terms of θ_w as $L\cos(\theta_w/2)$ where L is the element spacing in terms of wavelengths. Now as the path delay of a unit length affects the phase delay of any signal by its wave number, therefore for the above scenario, the resulting phase delay will be $kL\cos(\theta_w/2)$. For the discussion, let θ_b be the bend angle of the array where it can be expressed as a function of angle θ_w, given by,

$$\theta_b = \frac{(\pi - \theta_w)}{2}. \tag{2.18}$$

Then the phase delay between the signals received by the elements $A_{\pm 1}$ and $A_{\pm 2}$ can be expressed in terms of θ_b as $(kL\sin\theta_b)$. For the plane where the elements $A_{\pm n}$ are located, the phase delay between the signals received by $A_{\pm 1}$ and $A_{\pm n}$ will be as $(kL|n|\sin\theta_b)$. As the phase has being corrected here towards the source, therefore it will be additive in nature [29]. The expression in equation (2.19) is the phase difference between the adjacent antenna elements required to correct the ra-

diation pattern of the array placed on a wedge with a bend angle θ_b. The superscript w has been used to denote the case of wedge-shaped surface.

$$\Delta\phi_n^w = +kL|n|\sin\theta_b. \tag{2.19}$$

Apart from wedge shaped surfaces, a conformal array can also be realized on a singly curved surface such as a cylinder. Fig. 2.10 describes the position of the antenna elements placed on such a cylinder of radius r with its axis aligned with the $z-$axis. Then, the coordinate of the n^{th} element of the array can be denoted as (r, ϕ_n). Now by applying the same phase correction concept for the array placed on a wedge, the amount of required phase compensation can be computed as

$$\Delta\phi_n^c = +kr|\sin(\phi_n) - \sin(\phi_{n-1})|. \tag{2.20}$$

Again, the expression in (2.20) assumes a scan angle of $\phi_s = \pi/2$.

3. RESEARCH PROPOSAL

"*Imagination is more important than knowledge. For knowledge is limited, whereas imagination embraces the entire world, stimulating progress, giving birth to evolution. It is, strictly speaking, a real factor in scientific research.*"

— **Albert Einstein, "*Cosmic Religion and Other Opinions and Aphorisms*"**

3.1. Introduction

In this chapter, the research idea has been proposed along with a plan which clearly states the research questions that will be considered to answer in this dissertation. For conformal arrays, there are many properties of interest. Generally, when the surface of a typical planar antenna changes its shape to a non-planar orientation, the antenna loses its ability to radiate in a particular direction, as shown in Fig. 3.1. The desired direction of radiation may be broadside, i.e., normal to the axis of the array, or endfire, i.e., along the axis of the array. In this work, only broadside direction of radiation has been considered. Now, to achieve the broadside radiation in a conformal array, a number of challenges need to be taken care of. Much of the earlier work related to conformal antennas has not considered a number of fundamental questions that must be answered to overcome those challenges. The discussion in this chapter will try to lay out a path to answer several of those questions.

3.2. Research Interests and Questions

In general, spatial distributions of the array elements of a flexible array change when the surface of the antenna conforms from planar to any non-planar orientation. As shown in 3.2, all the elements of a 1×4 array (lying on the $x-y$ plane with its center at the origin) shifts to separate locations when the array conforms from planar ($AF_{\pm n}$: n^{th} array element from the origin while the array is flat) to a non-planar geometry ($AC_{\pm n}$: n^{th} array element from the origin while the array conforms to non-planar shape). Such alterations of the physical positions of conformal array elements force the array to create an unwanted and distorted radiation pattern [27]. Recently, several authors proposed multiple ways of correcting the radiation pattern of conformal phased array antennas by incorporating either the self-adapting beam scanning method [21] or the adaptive synthetic beam forming method [18]. However, most of these methods were limited to specific, non-planar, known

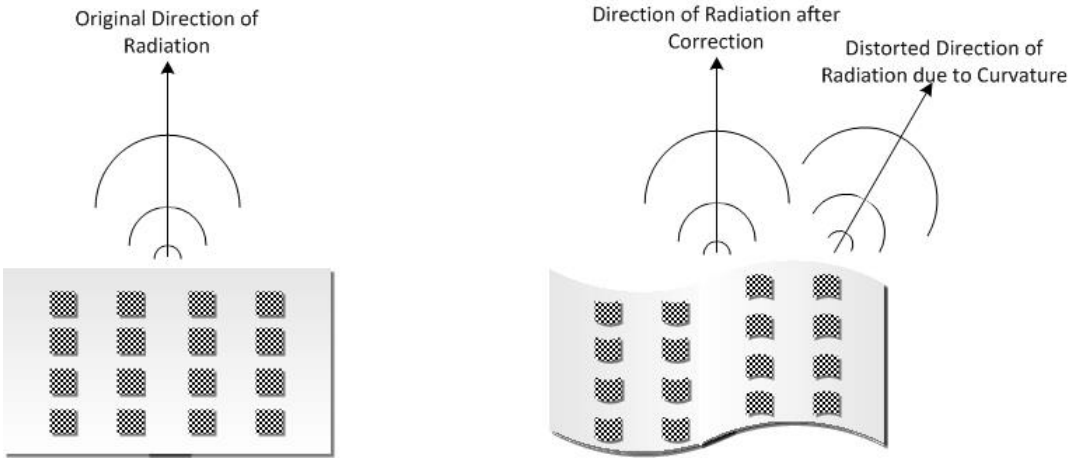

Figure 3.1. A microstrip antenna array on a planar surface and a multi-curved surface, respectively.

shapes with a single point of curvature, such as a wedge or a cylinder, and require the integration of a sizable sensor system with some complex analytical interface. Consequently, in the case of a flexible array placed on a conformal surface with more complex geometry, knowledge about the relative position of each element in real-time would be essential for computing the phase shifts required by the array elements for retaining the direction of maximum radiation. Hence, there remains an open avenue on the realization of conformal array antennas which not only can adapt to a wide variety of non-planar structures but also can correct itself (i.e., self-adapting) from resulting in an undesirable radiation pattern during run-time with a simple and low-profile phase correctional method. Therefore, the following three fundamental research questions can be summarized from the discussion above:

1. **How can a conformal surface with multiple points of curvature be analytically defined to compute the array factor expression of the array lying on that surface?**

2. **How can a sensor system be designed to integrate into the conformal surface without interfering with the performance of the array to sense the instantaneous change in surface curvature during run-time applications?**

3. **How can a computational algorithm be developed that will correct the array performance by selectively changing the phases of individual array elements in real-time while placed on a non-planar surface that may change shape with time?**

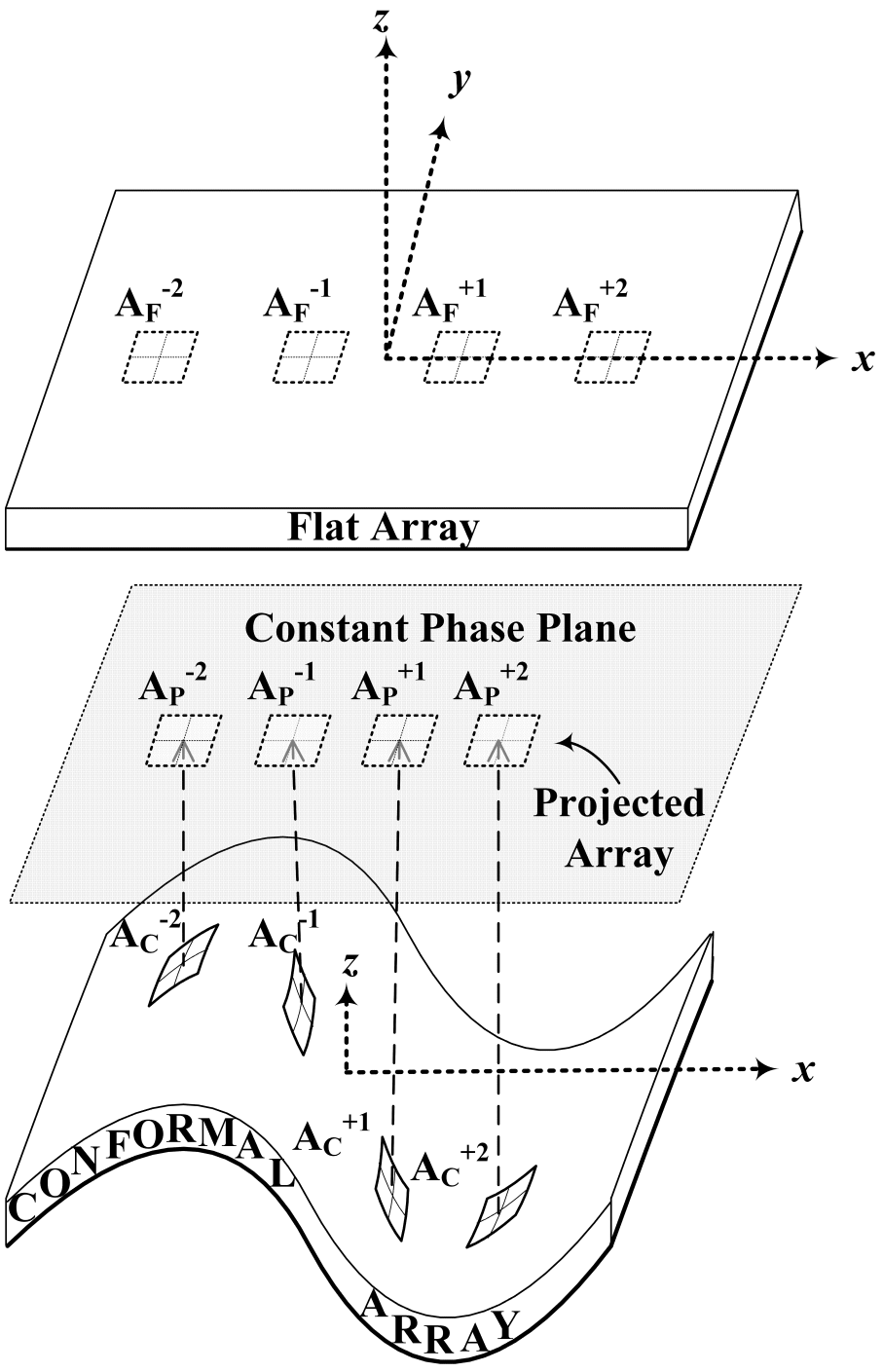

Figure 3.2. A Conformal Antenna Array: Virtual projection of the array elements to a constant phase plane in the x-y plane can be achieved (by following the arrow along the z-coordinates) when the flat array conforms to an arbitrary non-planar geometry.

3.3. Technical Objectives

Next, based on the above research questions, the following objectives have been formulated:

1. **Develop a new technique for computing the location of each antenna element in a conformal array antenna through geometric modeling.**
2. **Design a sensor network system for detecting the instantaneous change of the conformal surface in run-time applications.**
3. **Develop a real-time algorithm for correcting the array factor of the array through a feedback path to achieve the self-adapting capability.**

3.4. Research Outline

Based on the instantaneous spatial alignment of a conformal array, a real-time phase correction technique is reported here for the first time to achieve the self-adapting property of an array on a conformal surface with more than one curvature point. Additionally, by incorporating a novel sensor circuit system, the corresponding spatial information of array elements is used in real-time to evaluate the necessary phase correction for each array element. By feeding the calculated phase adjustments, all array elements are thus virtually projected to a new constant phase plane ($AP_{\pm n}$: n^{th} array element from the origin while the array is projected), as shown in Fig. 3.2. Furthermore, a comparative analysis of the proposed phase correction technique based on Spatial Movements of Antennas in Real-Time (**S.M.A.R.T.**), full-wave simulation, and laboratory measurements of field patterns for four different conformal arrangements of a 1×4 array antenna is presented. Finally, a study on the simulated and measured gain shift in the broadside direction of the array antenna during S.M.A.R.T. phase correction concludes the research.

3.5. Assumptions

The following assumptions have been made here. First, it is assumed that the individual elements of the conformal array do not change shape, only the array factor changes with the surface. Second, the effects of mutual coupling between the array elements are assumed to be negligible. Third, the sign convention of all angles with respect to the $x-y$ plane is positive during any rotation towards the $+z$ axis and negative during any rotation towards the $-z$ axis. Lastly, though all measurements were performed using a 1×4 phased array antenna resonating at 2.40 GHz, the reader

can extend the proposed method to design a conformal array antenna either with a different number of elements, or at other resonant frequencies, or via using different sensor systems by changing a few related parameters. However, the analytical approach in applying the **S.M.A.R.T.** phase correction technique should remain the same. Therefore, the idea presented in this research can be very useful for applications involving a conformal array antenna with complex geometries consisting of multiple points of curvature, such as skins of aircraft, spacesuits, and other vibrating and wearable surfaces.

4. GEOMETRICAL MODELING OF KNOWN CONFORMAL SURFACES USING BÉZIER CURVES

"*And it is the glory of geometry that it can perform so many things by so few principles derived from a foreign source.*"

— **Isaac Newton, "*Mathematical Principles of Natural Philosophy*"**

4.1. Introduction

At this point, it is assumed that the reader possesses some understanding on conformal phased array antennas. An important observation can be made now that a key component of the phase compensation technique using virtual projection method for any conformal array antenna is to know the location of each antenna element precisely on the conformal surface. The objective of this chapter is to present a new method for computing the location of each antenna element in a conformal array using a parametric curve, known as Bézier curves [30]. An example of a third-order Bézier curve is shown in Fig. 4.1. Then, the accuracy of the Bézier curves is shown by modeling problems with known surfaces and determining the pattern of a 1×4 conformal array on a wedge and a cylindrical-shaped surface in Fig. 4.2, and comparing the results to the values reported in [20].

4.2. Bézier Curves

In geometric modeling, the use of parametric equations to define complex curvatures is a very versatile and powerful scheme. For example, the work in [31] proposed a way to approximate an arbitrary shape by applying the concept of a special type of parametric equation, known as the Bézier curve, as shown in Fig. 4.1, to define a conformal cloak. More precisely, the analytical background of Bézier curves offers the flexibility of approximating different curved surfaces by selectively changing the values of coefficients, known as the weights, of control points in the parametric equations which define the related Bézier curve. For example, let us consider a two-dimensional, third-order Bézier curve with four defining control points (C_1, C_2, C_3, and C_4) on the $x-z$ plane, as shown in Fig. 4.1. In general, an n^{th} order Bézier curve consists of $(n+1)$ control points $(C_k: x_{C_k}, z_{C_k})$. The coordinates of the related control points are the coefficients of the following parametric equations which define the associated Bézier curve (x_{Bz}, z_{Bz}) in Fig. 4.1, where $(0 \leq t \leq$

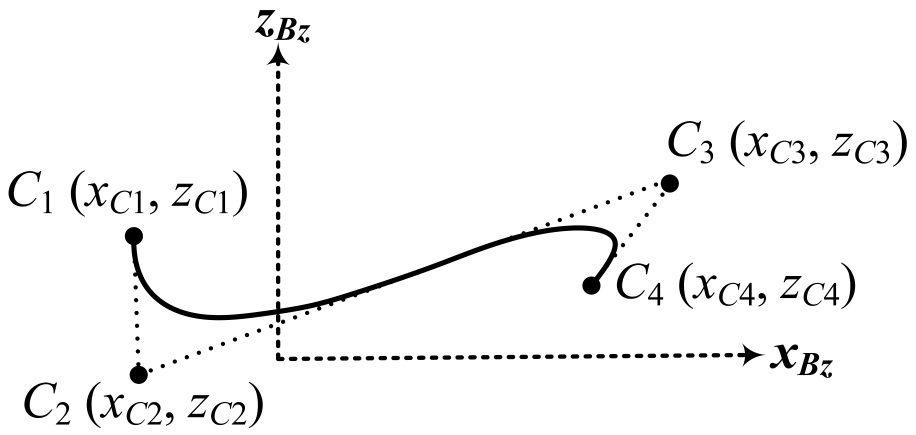

Figure 4.1. A third-order Bézier Curve, represented by the solid line, with four visible control points (C_1 through C_4) on the $x-z$ plane. The dotted line segments between the consecutive control points provide the reader a visual impression on the significance of the location of each control point.

1):

$$x_{Bz}(t) = (1-t)^3 x_{C_1} + 3t(1-t)^2 x_{C_2} + 3t^2(1-t)x_{C_3} + t^3 x_{C_4}, \tag{4.1}$$

and

$$z_{Bz}(t) = (1-t)^3 z_{C_1} + 3t(1-t)^2 z_{C_2} + 3t^2(1-t)z_{C_3} + t^3 z_{C_4}. \tag{4.2}$$

Next, it has been shown that the above pair of equations can then be used to mathematically approximate few known surfaces procured by a conformal array if the information on the inter-element spacing, number of elements, operating frequency, and the dimensions of the array elements are already known.

4.3. Approximating a Conformal Surface Shaped as a Wedge

First, the location of the elements in a 1×4 array on the wedge-shaped surface in Fig. 4.2(a) was computed using the Bézier curves. (A_{WN}: x_{WN}, z_{WN}) denotes the coordinates of the N^{th} array element on the wedge-shaped surface in Fig. 4.2(a). Each side of the wedge was first considered as a straight line and described using ($0 \le t \le 1$):

$$x(t) = (1-t)x_1 + tx_2, \tag{4.3}$$

and

$$z(t) = (1-t)z_1 + tz_2. \tag{4.4}$$

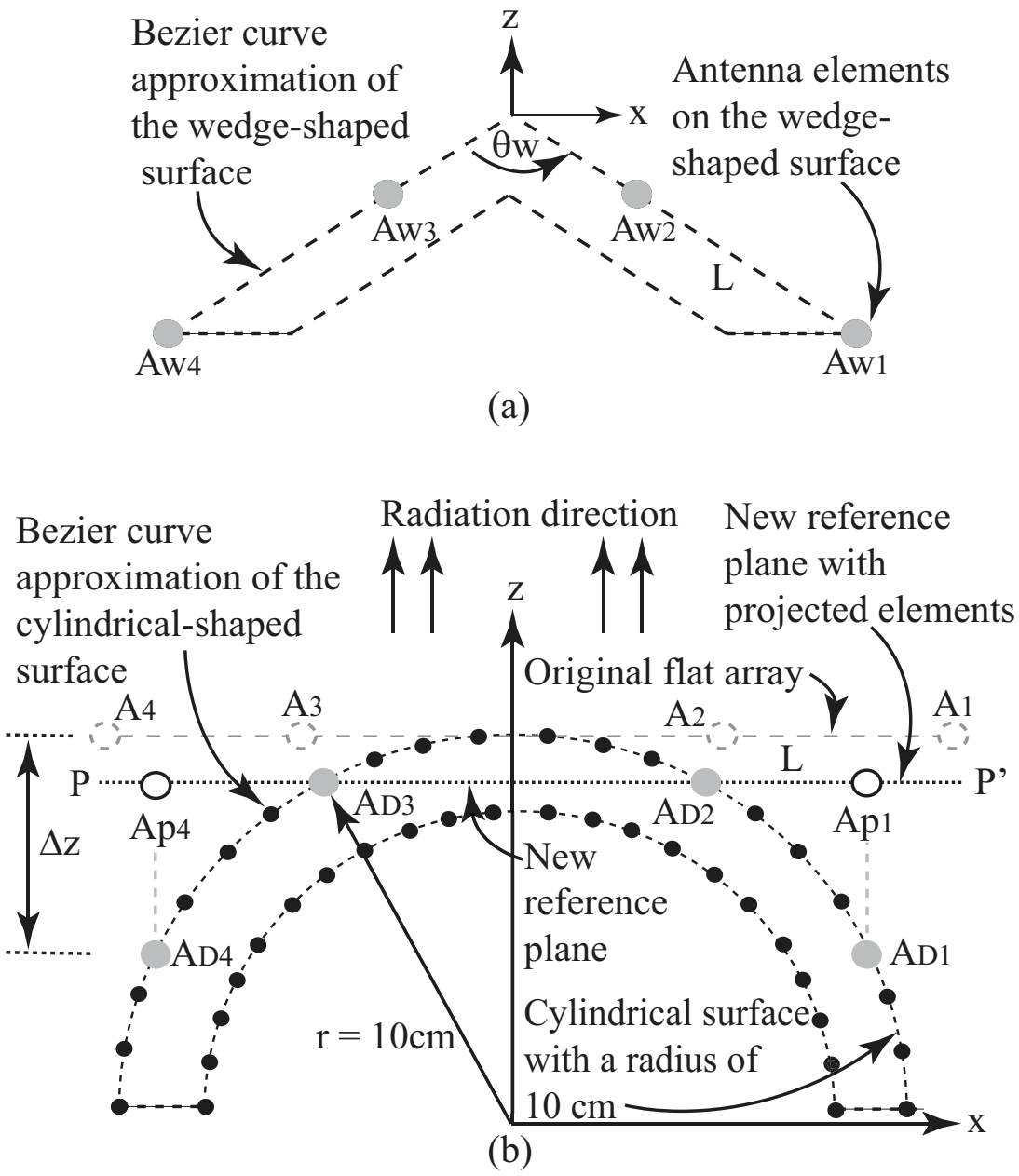

Figure 4.2. Four element antenna array on (a) wedge- and (b) cylindrical-shaped surfaces.

Next, considering the symmetry of the wedge with respective to the $z-$axis and the center of the wedge to be located at the origin, the left-half and right-half of the wedge are separately approximated by a pair of independent Bézier curves. To do so, the terms in (4.3) and (4.4) were equated to the terms in (4.1) and (4.2) with the same order to analytically solve for the location of control points of the Bézier curve. First, expanding (4.1) and (4.2) yields,

$$x_{B_z}(t) = t^3[x_{C_1} + 3x_{C_2} - 3x_{C_3} + x_{C_4}] + t^2[3x_{C_1} - 6x_{C_2} + 3x_{C_3}] + t[-3x_{C_1} + 3x_{C_2}] + x_{C_1}, \quad (4.5)$$

and

$$z_{B_z}(t) = t^3[z_{C_1} + 3z_{C_2} - 3z_{C_3} + z_{C_4}] + t^2[3z_{C_1} - 6z_{C_2} + 3z_{C_3}] + t[-3z_{C_1} + 3z_{C_2}] + z_{C_1}. \quad (4.6)$$

Then, by equating (4.5) to (4.3) and (4.6) to (4.4), the following sets of equations are obtained,

$$\left.\begin{aligned} &x_{C_1} = x_1, \\ &(-3x_{C_1} + 3x_{C_2}) = (-x_1 + x_2), \\ &(3x_{C_1} - 6x_{C_2} + 3x_{C_3}) = 0, \\ &(x_{C_1} + 3x_{C_2} - 3x_{C_3} + x_{C_4}) = 0, \end{aligned}\right\} \quad \text{for finding the } x- \text{ coordinates of the control points;} \quad (4.7)$$

and

$$\left.\begin{aligned} &z_{C_1} = z_1, \\ &(-3z_{C_1} + 3z_{C_2}) = (-z_1 + z_2), \\ &(3z_{C_1} - 6z_{C_2} + 3z_{C_3}) = 0, \\ &(z_{C_1} + 3z_{C_2} - 3z_{C_3} + z_{C_4}) = 0, \end{aligned}\right\} \quad \text{for finding the } z- \text{ coordinates of the control points.} \quad (4.8)$$

Now, one of the important properties of any Bézier curve is that the first and last control points of a Bézier curve are the initial and final points, respectively, of that curve. For a visual understanding, please check Fig. 4.1. Next, the following four careful considerations are made:

1. The origin represents the mid-point of the wedge-shaped surface, as shown in Fig. 4.2(a).

2. The initial points for both halves of the wedge are at the origin and their final points are

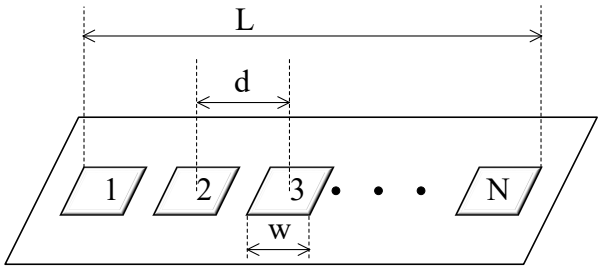

Figure 4.3. Geometry of a 1×N linear array antenna made of N identical rectangular patches (d=inter-element spacing, w=width of one patch antenna and L=length of the array).

therefore the two terminal points on either sides of the wedge-shaped surface.

3. The total length L of a $1 \times N$ linear array antenna made of N identical rectangular patches of width w with interelement spacing of d, as shown in Fig. 4.3, is

$$L = (N-1)d + w. \tag{4.9}$$

and

4. For simplicity, (x_1, z_1) and (x_2, z_2), which can be the coordinates of any two points on the wedge, are taken to be the initial and final points, respectively, for the two individual halves. Hence,

$$\left.\begin{aligned} x_1 &= 0 \\ z_1 &= 0 \end{aligned}\right\} \quad \text{coordinates of the initial point for the right-half of the wedge} \tag{4.10}$$

and

$$\left.\begin{aligned} x_2 &= \tfrac{L}{2} \times \sin\tfrac{\theta_w}{2} \\ z_2 &= -\tfrac{L}{2} \times \cos\tfrac{\theta_w}{2} \end{aligned}\right\} \quad \text{coordinates of the final point for the right-half of the wedge.} \tag{4.11}$$

Based on the above observations, the control points of the Bézier curve representing the right-half

section of the wedge are determined as follows,

$$C_1 : (x_{C_1}, z_{C_1}) = (0,0), \tag{4.12}$$

$$C_2 : (x_{C_2}, z_{C_2}) = (\frac{x_2}{3}, -\frac{z_2}{3}), \tag{4.13}$$

$$C_3 : (x_{C_3}, z_{C_3}) = (\frac{2x_2}{3}, -\frac{2z_2}{3}), \tag{4.14}$$

$$C_4 : (x_{C_4}, z_{C_4}) = (x_2, -z_2). \tag{4.15}$$

Similarly, the control points of the Bézier curve for the left-half section of the wedge are as follows,

$$C_1 : (x_{C_1}, z_{C_1}) = (0,0), \tag{4.16}$$

$$C_2 : (x_{C_2}, z_{C_2}) = (-\frac{x_2}{3}, -\frac{z_2}{3}), \tag{4.17}$$

$$C_3 : (x_{C_3}, z_{C_3}) = (-\frac{2x_2}{3}, -\frac{2z_2}{3}), \tag{4.18}$$

$$C_4 : (x_{C_4}, z_{C_4}) = (-x_2, -z_2). \tag{4.19}$$

The inter-element spacing of the four-element array was assumed to be $\lambda/2$, the operating frequency f was set to 2.47 GHz and the wedge angle was defined to be $\theta_w = 90^\circ$. This yields $N = 4$, $d \approx 63.4$ mm and $w = 43.6$ mm for a rectangular patch array [20] fabricated on a 20 mm thick and semi-flexible Rogers 6002 [32] substrate. Then the control points of the two curves are determined to be the following (in mm):

$$\left.\begin{aligned} C_1 &= (0,0), \\ C_2 &= (22.4, -22.4), \\ C_3 &= (44.8, -44.8), \\ C_4 &= (67.2, -67.2), \end{aligned}\right\} \quad \text{for the right-half of the wedge;} \tag{4.20}$$

and

$$\left.\begin{aligned} C_1 &= (0,0), \\ C_2 &= (-22.4, -22.4), \\ C_3 &= (-44.8, -44.8), \\ C_4 &= (-67.2, -67.2), \end{aligned}\right\} \quad \text{for the left-half of the wedge.} \tag{4.21}$$

Also, the list of the computed coordinates of the array elements on wedge is shown in column 3 of Table 4.1. The analytical values using trigonometry were computed for comparison and are reported in column 2 of Table 4.1 to show agreement.

Table 4.1. Coordinates of the array on the wedge-shaped surface.

Coordinates	Analytical (mm)	Bézier Curve (mm)
(x_{W1}, z_{W1})	(67.25,-67.25)	(67.25,-67.25)
(x_{W2}, z_{W2})	(22.52,-22.52)	(22.52,-22.52)
(x_{W3}, z_{W3})	(-22.52,-22.52)	(-22.52,-22.52)
(x_{W4}, z_{W4})	(-67.25,-67.25)	(-67.25,-67.25)

4.4. Approximating a Conformal Surface Shaped as a Cylinder

Next, the location of the elements in the array on the cylindrical-shaped surface shown in Fig. 4.2(b) were computed using the Bézier curves. $(A_{DN}: x_{DN}, z_{DN})$ denotes the coordinates of the N^{th} array element on the cylindrical-shaped surface in Fig. 4.2(b). Now, due to the technicality of any cylindrical surface, a cubic GC^2 approximation of Bézier curve representation of the surface was required [30] and will include some error. To perform this approximation, the surface of the array was again considered to be consists of two identical semi-circular arcs with a legth of $\frac{L}{2}$ on either sides of the $z-$axis and centered at the origin, as shown in Fig. 4.2(b). Now to construct the upper-right quarter of a circle that is centered at the origin and has a radius = r, using a third-order Bézier curve by the GC^2 approximation method, the coordinates of the four control points of the curve are shown in 4.4 and evaluated using following equations [33]:

$$C_1: (x_{C_1}, z_{C_1}) = (0, r), \tag{4.22}$$

$$C_2: (x_{C_2}, z_{C_2}) = (\kappa \times r, r), \tag{4.23}$$

$$C_3: (x_{C_3}, z_{C_3}) = (r, \kappa \times r), \tag{4.24}$$

$$C_4: (x_{C_4}, z_{C_4}) = (r, 0), \tag{4.25}$$

where

$$\kappa = 4(\frac{\sqrt{2}-1}{3}). \tag{4.26}$$

Based on the above observations, the control points of the Bézier curve representing the right-half

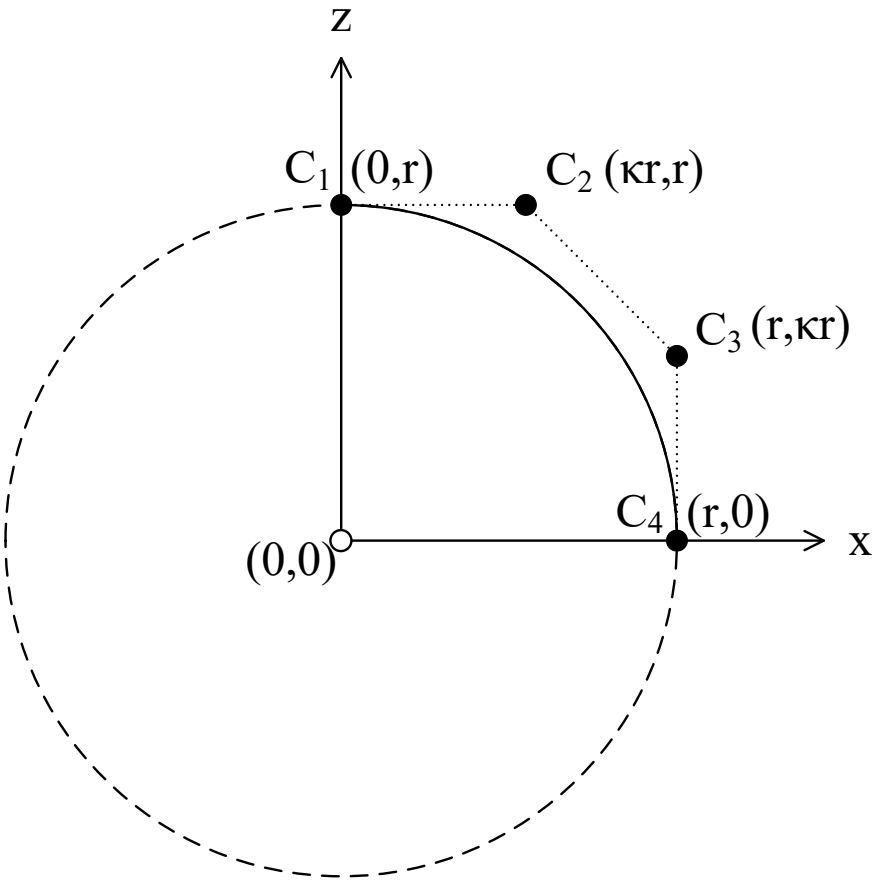

Figure 4.4. Construction of the upper-right quarter of a circle of radius r using a third-order Bézier curve by the GC^2 approximation method. The locations and coordinates of the associated four control points are given for a better understanding.

section of the cylindrical surface are determined as follows,

$$C_1 : (x_{C_1}, z_{C_1}) = (0, r), \tag{4.27}$$

$$C_2 : (x_{C_2}, z_{C_2}) = \left(4(\frac{\sqrt{2}-1}{3})r, r\right), \tag{4.28}$$

$$C_3 : (x_{C_3}, z_{C_3}) = \left(r, 4(\frac{\sqrt{2}-1}{3})r\right), \tag{4.29}$$

$$C_4 : (x_{C_4}, z_{C_4}) = (r, 0). \tag{4.30}$$

Similarly, the control points of the Bézier curve for the left-half section of the cylindrical surface are as follows,

$$C_1 : (x_{C_1}, z_{C_1}) = (0, r), \tag{4.31}$$

$$C_2 : (x_{C_2}, z_{C_2}) = \Big(-4(\frac{\sqrt{2}-1}{3})r, r \Big), \tag{4.32}$$

$$C_3 : (x_{C_3}, z_{C_3}) = \Big(-r, 4(\frac{\sqrt{2}-1}{3})r \Big), \tag{4.33}$$

$$C_4 : (x_{C_4}, z_{C_4}) = (-r, 0). \tag{4.34}$$

Again, the inter-element spacing of the four-element array was assumed to be $\lambda/2$, the operating frequency f was set to 2.47 GHz and the radius of the cylindrical surface was defined to be $r = 10$ mm. This yields $N = 4$, $d \approx 63.4$ mm and $w = 43.6$ mm for a rectangular patch array [20] fabricated on a 20 mm thick and semi-flexible Rogers 6002 [32] substrate. Then the control points of the two curves are determined to be the following (in mm):

$$\left.\begin{aligned} C_1 &= (0, 0), \\ C_2 &= (55.2, 0), \\ C_3 &= (100, -55.2), \\ C_4 &= (100, -100), \end{aligned}\right\} \text{ for the right-half of the cylindrical surface;} \tag{4.35}$$

and

$$\left.\begin{aligned} C_1 &= (0, 0), \\ C_2 &= (-55.2, 0), \\ C_3 &= (-100, -55.2), \\ C_4 &= (-100, -100), \end{aligned}\right\} \text{ for the left-half of the cylindrical surface.} \tag{4.36}$$

The computed location of each antenna element is shown in column 3 of Table 4.2. Again, for comparison, the location of each antenna element was computed using trigonometry and is shown in column 2 of Table 4.2. Also, the shape of the cylindrical surface was computed analytically and using the Bézier curves. These results are shown in Fig. 4.5, and it is shown that the Bézier curves can be used to accurately model the cylindrical surface. Finally, the phase-compensated [20] pattern of the 1×4 array on the cylindrical surface described by the Bézier curves was computed and compared to the results reported in [20]. A good comparison between these results is shown

in Fig. 4.6; indicating that the Bézier curves presented here can be used to accurately design a self-adapting conformal array that uses the phase-compensation technique described in [20].

Table 4.2. Coordinates of the array on the cylindrical-shaped surface.

Coordinates	Analytical (mm)	Bézier Curve (mm)
(x_{D1}, z_{D1})	(79.0, -38.69)	(79.0, -43.14)
(x_{D2}, z_{D2})	(29.89, -4.57)	(29.89, -5.45)
(x_{D3}, z_{D3})	(-29.89, -4.57)	(-29.89, -5.45)
(x_{D4}, z_{D4})	(-79.0, -38.69)	(-79.0, -43.14)

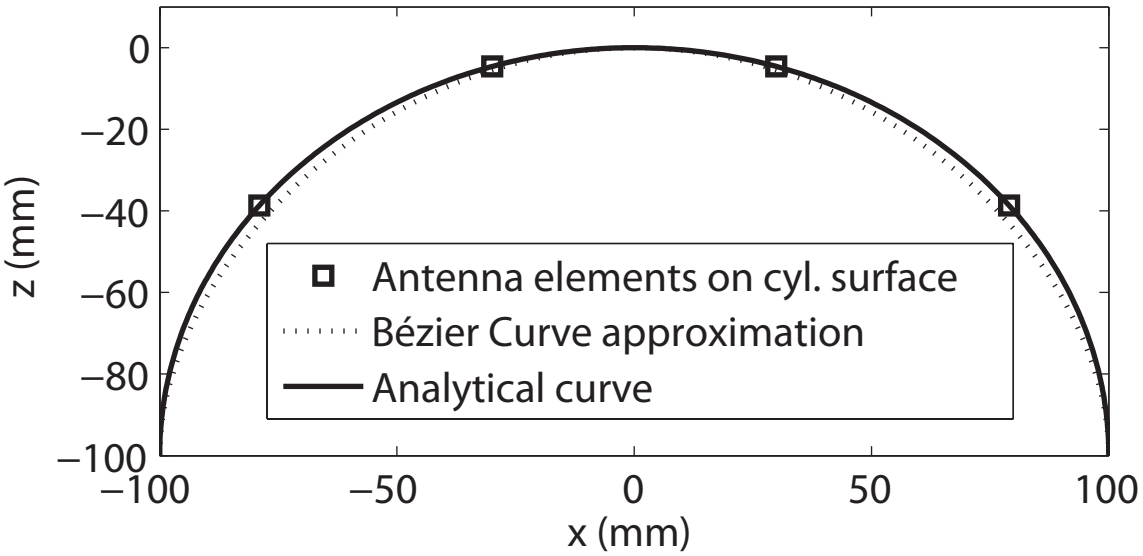

Figure 4.5. Comparison between the cylindrical surface computed using analytical methods and the Bézier curves.

4.5. Conclusion

A new technique for determining the shape of a wedge- and cylindrical-shaped surface was presented here. In particular, a pair of third-order Bézier curves were used to compute the location of the antenna elements on these surfaces and then this information was used to implement a phase-compensation technique for radiation pattern recovery. Finally, computations were validated with a comparison to analytical and published results [34].

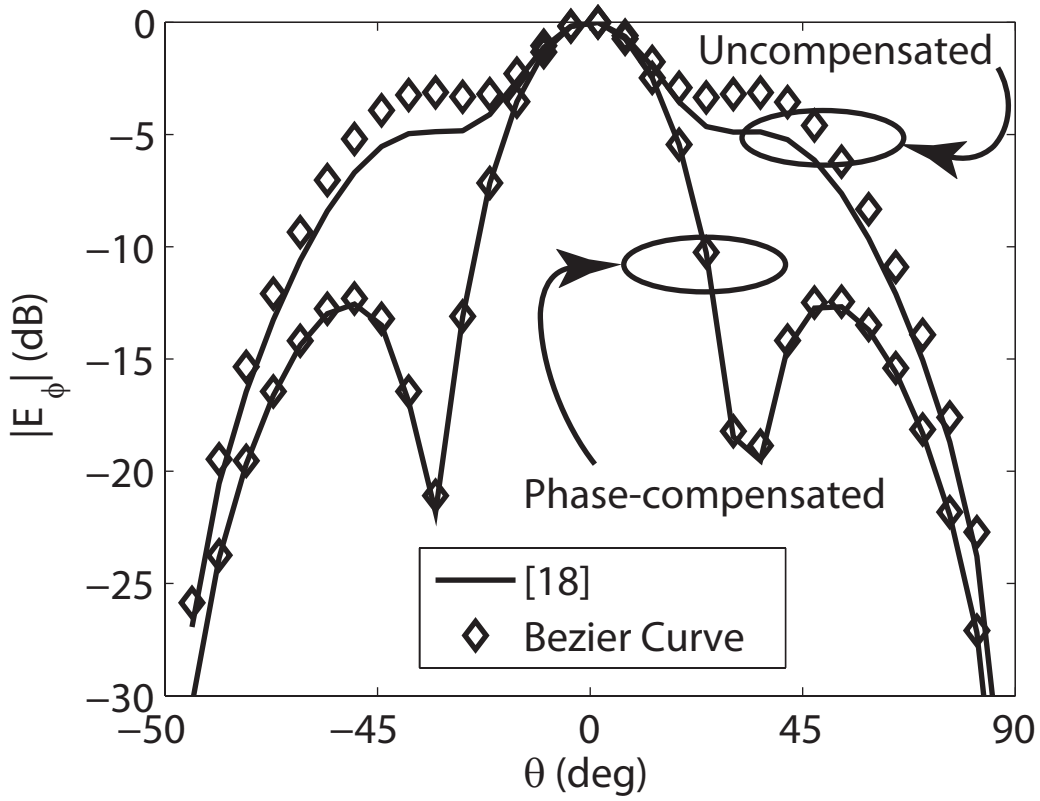

Figure 4.6. Normalized uncompensated and phase-compensated patterns.

5. SENSING THE RELATIVE DISPLACEMENTS OF THE ELEMENTS IN A CONFORMAL ARRAY ANTENNA IN REAL-TIME

"*First, it is necessary to study the facts, to multiply the number of observations, and then later to search for formulas that connect them so as thus to discern the particular laws governing a certain class of phenomena. In general, it is not until after these particular laws have been established that one can expect to discover and articulate the more general laws that complete theories by bringing a multitude of apparently very diverse phenomena together under a single governing principle.*"

— Augustin Louis Cauchy

5.1. Introduction

In electromagnetic wave propagation, the three-dimensional surface constituted by electromagnetic waves of an identical phase is known as a wavefront. At any instant, all the elements of a flat planar array, if oriented as shown in Fig. 5.1, will receive an electromagnetic wave from the $+z$-direction in equal phase. However, for a conformal array antenna, as shown in Fig. 5.2, the array elements may receive an electromagnetic wave from the $+z$-direction in different phases at any instant due to their non-planar alignment. Thus, the real-time positions of the array elements govern the instantaneous phase of the signal they receive. Therefore, to incorporate the projection method discussed in the previous chapter, a sensor system is then required to know the instantaneous location of individual array elements in designing a conformal array antenna. Moreover, a feedback control circuit may supplement the sensor system to provide necessary phase corrections to each array element in a conformal array antenna through parallel phase shifters. By using the resistive sensors and phase compensation technique reported in [20], an analytical approach to the designing of a universal control circuit for conformal arrays was reported in the first section of this chapter. Additionally, the following section of this chapter presents how the limitations of the aforementioned resistive sensor circuit have inspired to adopt a novel way in using a completely different type of sensor system for implementing real-time phase compensation in non-planar conformal arrays.

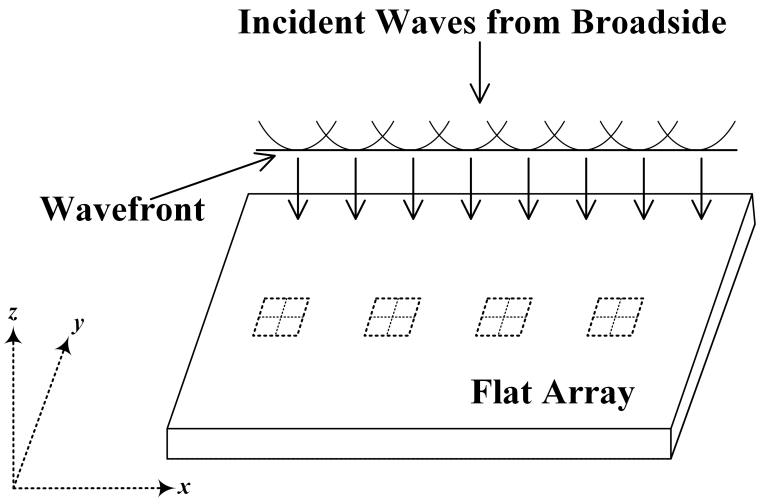

Figure 5.1. A flat planar array is receiving an electromagnetic wave, propagating from the $+z$-direction.

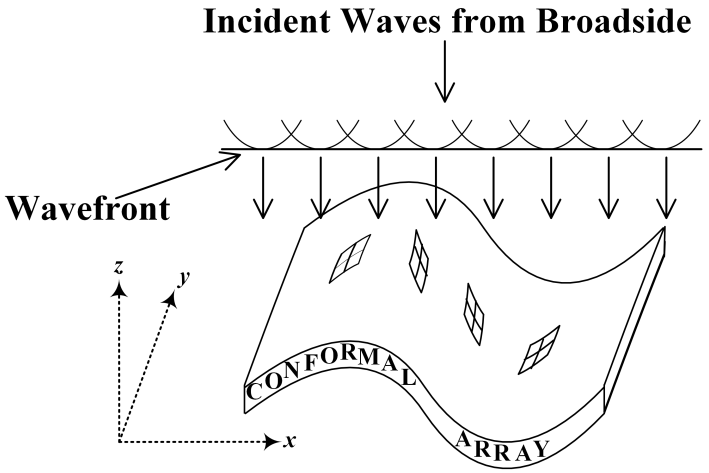

Figure 5.2. A conformal planar array is receiving an electromagnetic wave, propagating from the $+z$-direction.

5.2. On Designing a Universal Control Circuit for Phase Compensation Technique in Self-Adapting Flexible (SELFLEX) Antenna Array

Earlier work featured autonomous correction of conformal array antennas for real-time applications using various types of analog strain sensors [20], [35]. However, the idea of incorporating a universal control circuit, instead of using different control circuits for different sensors, has not yet been explored. The objective of this analytical study is to propose a technique of designing a generic control circuit that can be used along with many different kinds of analog sensors to provide autonomous phase compensation for a conformal array.

5.2.1. Theory

One of the challenges in designing a self-adapting conformal array is to retain its original direction of radiation irrespective of its curvature of surface in real time. One technique to overcome such issue is to adjust the array performance at any instant by sensing changes in the surface of the array and adjusting the phase of the voltages driving each element in the array (i.e., autonomous phase compensation). For this work, the 1×4 array on the wedge-shaped surface shown in Fig. 5.3 was considered. The antenna elements are denoted as A_1, A_2, A_3 and A_4. The array in the flat position is shown along the line with the solid box. Then, the array on the wedge-shaped surface with angle θ_w is illustrated with the elements in the wedge-shaped box with the dotted lines. Also, for this work, the direction of radiation is assumed to be in the $+z$-direction. Therefore, one method of supporting radiation in the $+z$-direction when the array is flat (i.e., outlined by the box with the solid line) is to drive each element with the same phase. However, when the array is on the wedge-shaped surface and each element is driven with the same phase, the main lobe moves away from the $+z$-direction in an undesired manner. One method to move the radiation back to the $+z$-direction is to introduce a positive phase on the voltage driving elements A_{w1} and A_{w4}. This positive phase will then cancel some of the negative propagation phase and will result in a field radiated from A_{w1} and A_{w4} that will arrive at the reference plane P in Fig. 5.3 with the same phase as the fields radiated from elements A_{w2} and A_{w3}, thus resulting in broadside radiation [20]. As an example, in Fig. 5.3, a 1×4 planar conformal array, shown as solid line, was assumed to take a shape of a wedge of angle θ_w, shown as a dotted line.

In an earlier work [20], it has been shown that a simple circuit consisting of flexible strain resistive sensor, as shown in Fig. 5.5, an instrumentation amplifier and an array of voltage controlled analog phase shifters can be used to insert proper phasor voltages to selected array elements

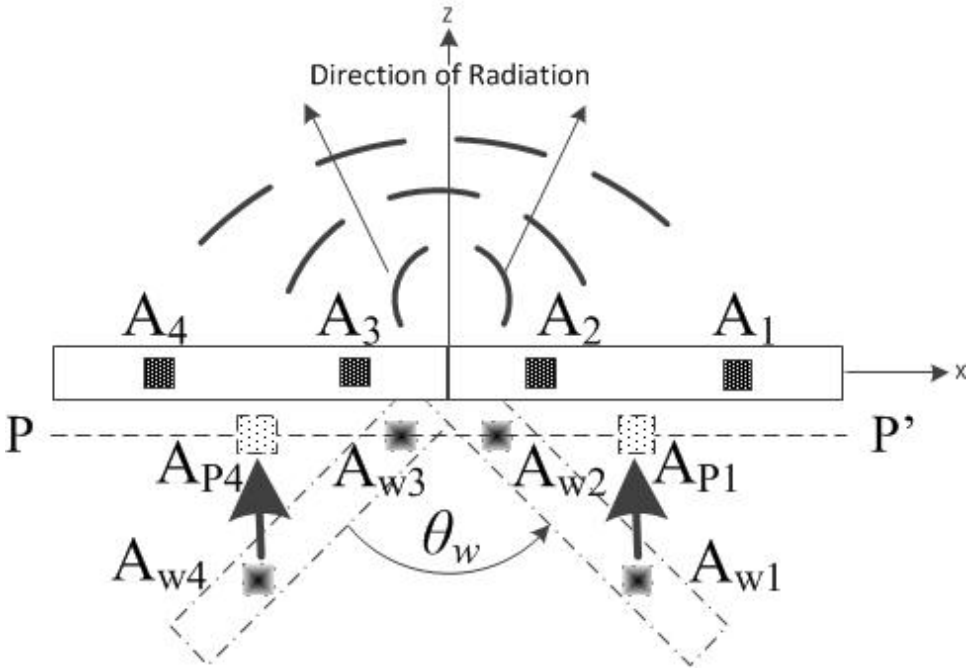

Figure 5.3. A 1×4 conformal antenna array on planar and wedge shaped surfaces.

based on their physical locations to retain the direction of maximum radiation of any singly curved conformal array. However, other than maintaining the maximum direction of radiation, a conformal antenna can also be used for beam forming at any particular direction. For an example, unlike the required phasor voltages on each array element for beam forming technique, the required phasor voltages for maintaining maximum direction of radiation of a conformal array will be different. Earlier reported sensor control circuits shown in Fig. 5.4 [20]-[21], that converts the sensor output to a required phasor control voltage, uses an instrumentation amplifier (Analog Devices AMP04). Considering the versatile application of conformal array antenna, if the sensor control circuit can be used as a universal solution, then an analytic technique is required. Based on the choice of the user for obtaining different a amount of phases at different orientation of the conformal array, this analytic technique can then be used to evaluate the value of the necessary circuit components, such as pull up resistor R_1, gain controlling resister R_{gain}, driving voltage V_{cc} and $-V_{cc}$, and reference voltage V_{ref} to obtain the desired phase shifter control voltage V_{ctrl}, as shown in Fig. 5.4.

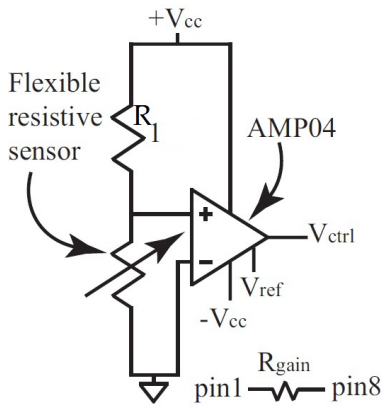

Figure 5.4. Schematic of the control circuit to drive phasor voltages in conformal array elements

5.2.2. Derivation

According to the data-sheet of instrumentation amplifier AMP04, the following equation of the output V_{ctrl} can be expressed considering the circuit connection depicted in Fig. 5.4,

$$V_{ctrl} = \frac{100V_{cc}}{R_{gain}}\left(\frac{R_{sensor}}{R_1 + R_{sensor}}\right) + V_{ref} \tag{5.1}$$

where all resistors are in $k\Omega$ magnitude, and R_{sensor} is the variable resistor output of the sensor based on the curvature of the surface of the array. Now from the measurement reported in [20]-[21], the relation between R_{sensor} and the bend angle of the wedge θ_w in degrees can be expressed as,

$$R_{sensor} = f(\theta_w) = \frac{6}{35}|\theta_w| + 16. \tag{5.2}$$

Next, the derivation to find the values of the unknowns in the control circuit is shown. Depending on the maximum voltage swing required by the user, V_{cc} can be chosen accordingly to avoid reaching saturation in the output. Now, from three phase compensating control voltage values, v_1, v_2, v_3 required by the user for three different bend angles θ_{w1}, θ_{w2}, θ_{w3} of the conformal array, the three unknowns R_1, R_{gain}, R_{sensor} can be evaluated. Applying KVL and KCL in equations

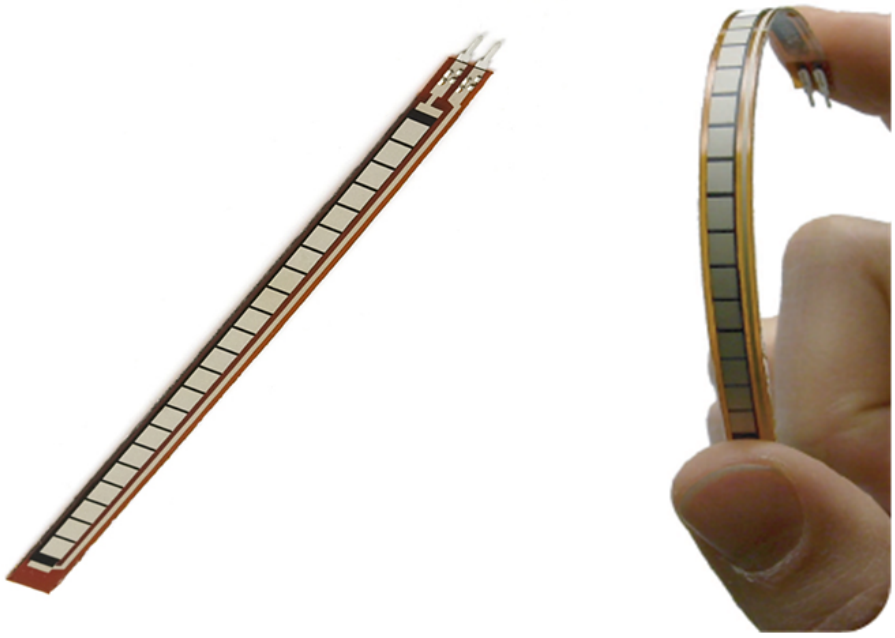

Figure 5.5. Flexible Resistive Strain Sensor, **Flex Sensor FS** (image taken from the manufacturer's (*Spectra Symbol*) datasheet.)

5.1-5.2 yield following quadratic equation from where R_1 can be solved from the larger root but ignoring the sign:

$$R_1{}^2 a + R_1 b + c = 0 \tag{5.3}$$

where

$$p = \frac{1}{100}\left(\frac{v_3 - v_2}{f(\theta_{w3}) - f(\theta_{w2})}\right), \tag{5.4}$$

$$q = \frac{1}{100}\left(\frac{v_2 - v_1}{f(\theta_{w2}) - f(\theta_{w1})}\right), \tag{5.5}$$

$$a = p - q, \tag{5.6}$$

$$b = f(\theta_{w2})a + f(\theta_{w3})p - f(\theta_{w1})q, \tag{5.7}$$

$$c = f(\theta_{w1})f(\theta_{w2})a \tag{5.8}$$

Next, R_{gain} can be solved from:

$$R_{gain} = \frac{100}{G} \tag{5.9}$$

where

$$r = \frac{f(\theta_{w2})}{R_1 + f(\theta_{w2})} - \frac{f(\theta_{w1})}{R_1 + f(\theta_{w1})}, \tag{5.10}$$

and

$$G = \frac{r(v_2 - v_1)}{100}. \tag{5.11}$$

Lastly, V_{ref} can be determined as:

$$V_{ref} = v_1 - 100G\left(\frac{f(\theta_{w1})}{R_1 + f(\theta_{w1})}\right). \tag{5.12}$$

5.2.3. Result and Verification

For verification of the proposed technique, three angles $\theta_{w1} = 0°$, $\theta_{w2} = 30°$, and $\theta_{w3} = 45°$ have been chosen. Based on the SELFLEX design reported in [20], three output voltages for phase controller circuit have been chosen as 3.6 volt, 5.45 volt, and 6.5 volt. Considering $V_{cc} = 15$ volt, the evaluated values of the circuit components are found to be $R_1 = 98.5k\Omega$, $R_{gain} = 30k\Omega$, and $V_{ref} = -3.4$ volt. Then these values have fed to SPICE model for simulation and the following Table 5.1 shows a very good comparison between user required and simulated values using the proposed analytical values.

Table 5.1. Comparison between analytic and simulated values

Angle of Wedge	Analytic Value	Simulated Value	Normalized Phase
$\theta_w = 0°$	3.6 volt	3.63 volt	$0°$
$\theta_w = 30°$	5.45 volt	5.49 volt	$61°$
$\theta_w = 45°$	6.5 volt	6.36 volt	$96°$

5.2.4. Discussion

In this section, a new technique to evaluate the circuit components of a universal control circuit for the phase compensation technique in a self-adapting conformal phased array antenna has

been proposed. From a designing perspective, the evaluated values using the proposed technique for a known case of conformal arrays has been compared with simulated values and the results show a very good match.

5.2.5. Limitations of the Resistive Sensor Circuit

Although the resistive sensor circuit works well to sense the curvature of a singly curved surface like wedge or cylinder, however it fails in the presence of multiple curvatures on its surface, e.g. S-shaped surface. Moreover, the resistive sensor yields outputs of low-precision. It is also very frail in nature and thus requires delicate handling. Hence, a better and more reliable sensor system is now required to design self-adaptable conformal arrays that may take any shape during an application.

5.3. Choosing a Good Sensor System

It was indeed a difficult task to select a good sensor system that will be an optimum choice for the current work. Several factors were considered before making a final decision. The sensor should be compact, agile, mechanically rugged, low-profile, low-cost, easy to install, equipped with a simpler interface for control operation, and able to sense the geometrical orientation based on its location. Out of many options currently available in the market, a conclusion was reached after several months of research to use a special kind of sensor known as the *Inclinometer*.

5.4. Inclinometer

An inclinometer, with the help of earth's gravity (g), can sense any physically applied inclination from a reference position and outputs an equivalent change in voltage. Unlike an accelerometer which produces an output only during an event of movement, the inclinometer has the advantage of yielding a constant output based on its true inclination and thus does not require any additional circuitry to hold the instantaneous output data. The inclinometer sensors used here, shown in Fig. 5.6, were manufactured by *Murata Electronics* (Part No: SCA100T) [36] and had a resolution of 0.0025° and an accuracy of $35mV/^\circ$. It can instantaneously detect a relative inclination in all directions from -90° to $+90^\circ$ which makes this sensor very suitable for the current work. As shown in Fig. 5.7, the used inclinometer module is an upgraded version that includes a protective housing (Part No: SCA121T). This version of the sensor comes with an integrated, user-friendly interface that provides the sensor a firm mechanical grip which precisely eliminates the occurrence of damped vibration while the sensor initiates or ceases a movement. The output voltages of the inclinometer during inclinations respective to a single axis (the y–axis) from -50° to $+50^\circ$ with a step of unit degree

Figure 5.6. Inclinometer Sensor, **SCA100T** (image taken from the manufacturer's (*Murata Manufacturing*) datasheet.)

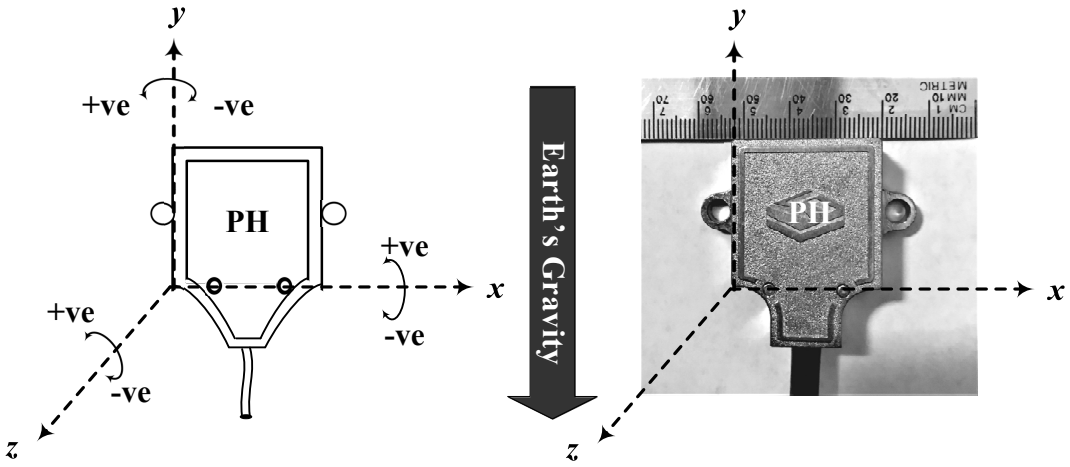

Figure 5.7. On the left, the positive and negative inclinations of the inclinometer sensor in all three coordinates have been defined. On the right, an actual image of the sensor including the Protective Housing (PH) *SCA121T* is provided for reference.)

are shown in Fig. 5.8. The alignment of the inclinometer in Fig. 5.7 is considered as the 0° inclination in all three coordinates. A very good agreement between the expected and measured sensor data validates the use of the inclinometer in this project without any loss of generality. Hence, when these identical inclinometers would be methodically placed along with the array elements, any conformal application resulting in a non-planar orientation of the array can be instantaneously detected from the cumulative responses of the sensors. Inspired by that, the next chapter discusses on using the sensor data for measuring the relative spatial displacements of array elements in a 1–by–N conformal array antenna.

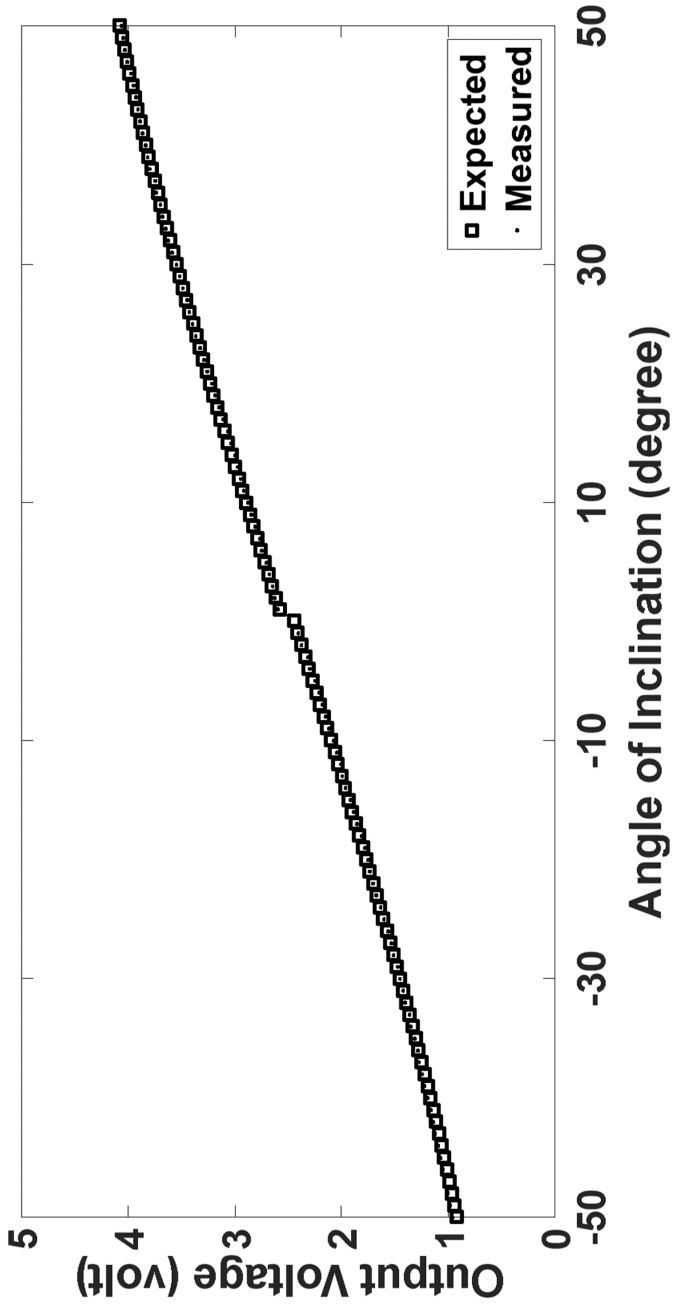

Figure 5.8. The output voltage of an inclinometer module at different angle of inclinations around the axis of rotation. Test Settings: $V_{ref} = 2.50$ V, $V_{cc} = 5$ V, axis selected for the applied inclination: $y-$axis.)

6. REAL-TIME SENSING AND GEOMETRICAL MODELING OF UNKNOWN CONFORMAL SURFACES

"*Every existence above a certain rank has its singular points; the higher the rank the more of them. At these points, influences whose physical magnitude is too small to be taken account of by a finite being may produce results of the greatest importance.*"

— James Clerk Maxwell

6.1. Introduction

In this chapter, the method of geometrical modeling of conformal surfaces with an unknown shape by locating relative displacements of elements under conformal applications is developed. Simultaneously, the technique to incorporate a real-time sensor system to detect the change of shape of the conformal surface is investigated. Inspired by the work reported so far, this chapter discusses on details of the novel **S.M.A.R.T.** phase correction technique for a 1–by–N conformal array antenna.

6.2. Spatial Movements of Antennas in Real-Time (S.M.A.R.T.) for Conformal Applications

Let us consider a linear 1–by–N array on the x–y plane, with its direction of maximum radiation towards broadside, i.e., normal to the x–y plane and towards the $+z$ direction, as shown in Fig. 6.1. The elements of the array are identical and have a rectangular shape with length l along the y–axis and width w along the x–axis. The elements are separated from each other by an inter-element spacing of d along the x–axis. Now, for providing some mechanical support to integrate the inclinometer sensors with the array, every array element is considered resting on a rectangular platform that consists of a chamber where an individual inclinometer module can physically fit, as shown in Fig. 6.1. These supporting platforms are identical and independent of each other during an event of displacement under any conformal application. The dimensions of these supporting platforms can be determined based on the size of the sensor modules and the array elements. The height P_Z along the z–axis and the length P_Y along the y–axis of the supporting platforms are governed by height and length of the inclinometer module, respectively. The width P_X along the x–axis of the platforms is determined by the inter-element spacing d and the width of the array elements w where $w \leq P_X < d$. Let us now consider the possibility of the non-planar orientations of

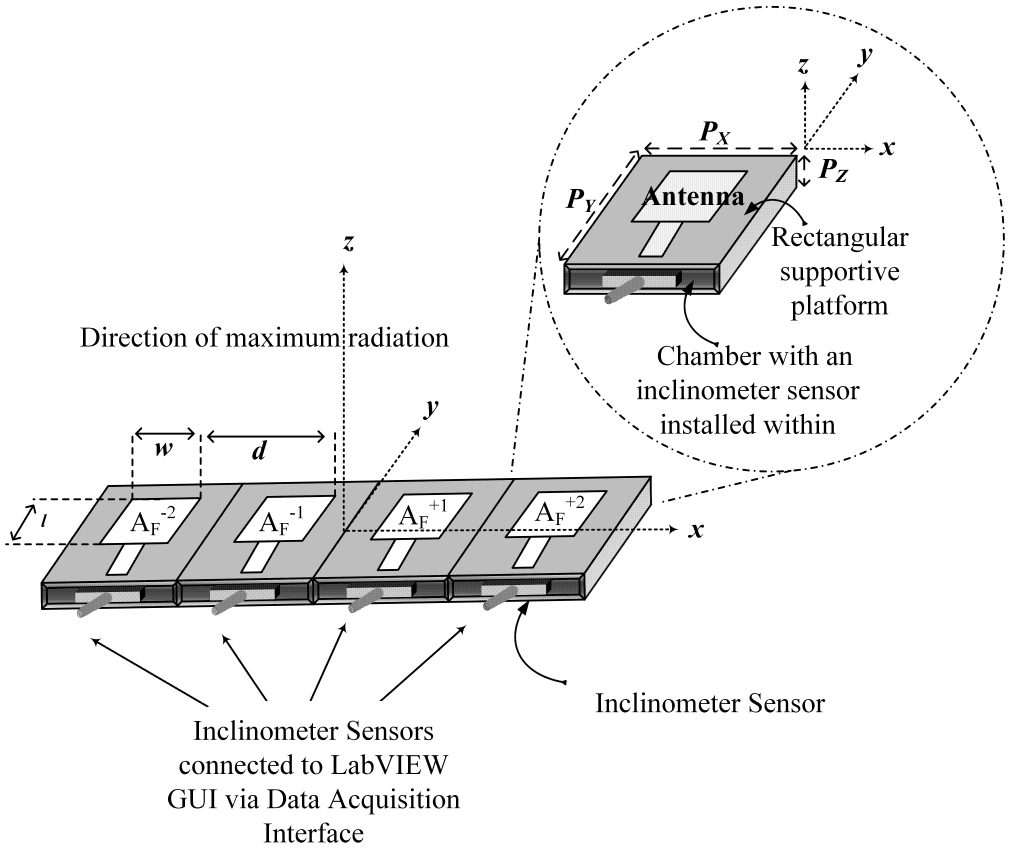

Figure 6.1. A linear planar 1 – by – 4 array on the $x-y$ plane radiating towards the $+z$ direction. An enhanced description of the supporting platform and the chamber is included for convenience.

the array. As the surface of the array conforms from planar to a non-planar alignment, proper phase correction to individual array elements will then be required for retaining the maximum direction of radiation. Let us again presume the array is aligned along the x–y plane, radiating to the broadside (towards the $+z$–direction), and able now to perform any rotational movement in the direction to the $\pm z$ axes with respective to the x–y plane, as shown in Fig. 6.2. Under such circumstances, the x– and z– coordinates of all the array elements would change while the associated y– coordinates remain preserved.

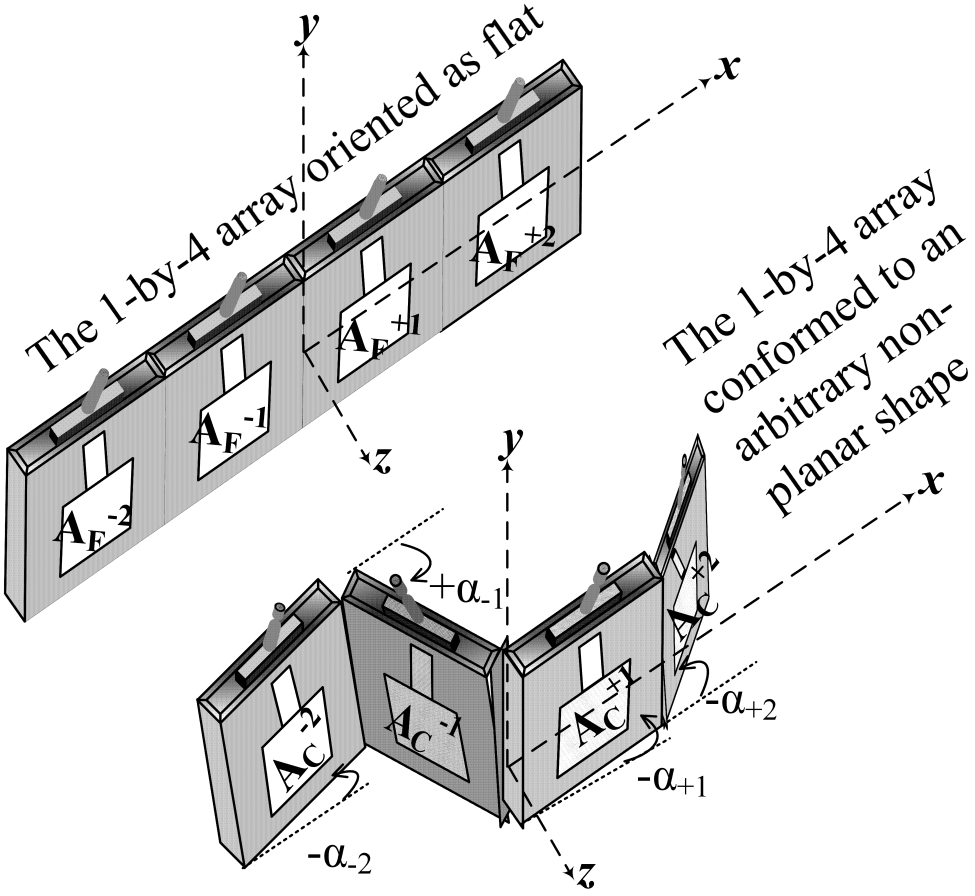

Figure 6.2. Rotational movements of the array elements during a non-planar conformal application. For reference, the equivalent planar (flat) orientation and the sign convention of the angles during conformal applications are provided.

6.3. A Sensor System for Real-Time Conformal Applications using S.M.A.R.T.

The connected inclinometer sensors have the significant role here of distinctly measuring the angular displacements of individual array elements in the occurrence of any rotational movement in the direction to the $\pm z$ axes with respective to the x–y plane. For simplicity of the discussion, $N = 4$ is chosen. Let us now define the following x– and z– coordinates from Fig. 6.2:

1. the center of the $\pm k^{\text{th}}$ element of the array: $(x_{\pm k}, y_{\pm k}, z_{\pm k})$;
2. the center of the array: $(0, 0, 0)$;
3. measure of the rotational movement of the k^{th} element in the direction to the $\pm z$ axes with respective to the x–y plane: $\pm\alpha_k$, where positive and negative signs respectively follows the positive and negative (y axis) inclinations as defined in Fig. 5.7.

Then from geometry, the following generic equations yield the new x– and z– coordinates of the centre of the $\pm k^{\text{th}}$ array element $(x'_{\pm k}, z'_{\pm k})$ due to the non-planar conformal application:

$$x'_{\pm k} = \pm[(k\text{–}1) \times (P_x \cos\alpha_{\pm(k-1))})] \pm [(k \times d)\text{–}(P_x(k\text{–}1)\text{–}0.5d) \cos\alpha_{\pm k}] \tag{6.1}$$

and

$$z'_{\pm k} = \pm[(k\text{–}1) \times (P_x \sin\alpha_{\pm(k-1))})] \pm [(k \times d)\text{–}(P_x(k\text{–}1)\text{–}0.5d) \sin\alpha_{\pm k}]. \tag{6.2}$$

Next, a reference element m $(1 \leq m \leq N)$ is chosen via the following constraint:

$$\max(z'_{\pm k}, \forall k) = z_m. \tag{6.3}$$

Followed by that, the z–plane contained by this m^{th} element is selected as the reference plane, and the relative z–coordinate displacement of the $\pm k^{\text{th}}$ array element $(z'_{\pm k})$ is measured with respect to the chosen reference plane for all values of k where

$$\Delta z_{\pm k} = (z_m\text{–}z'_{\pm k}), \ \forall k. \tag{6.4}$$

Now if λ denotes the associated wavelength, then by using the following relation:

$$\text{Phase Difference} = \left(\frac{2\pi}{\lambda}\right) \times (\text{Path Difference}), \tag{6.5}$$

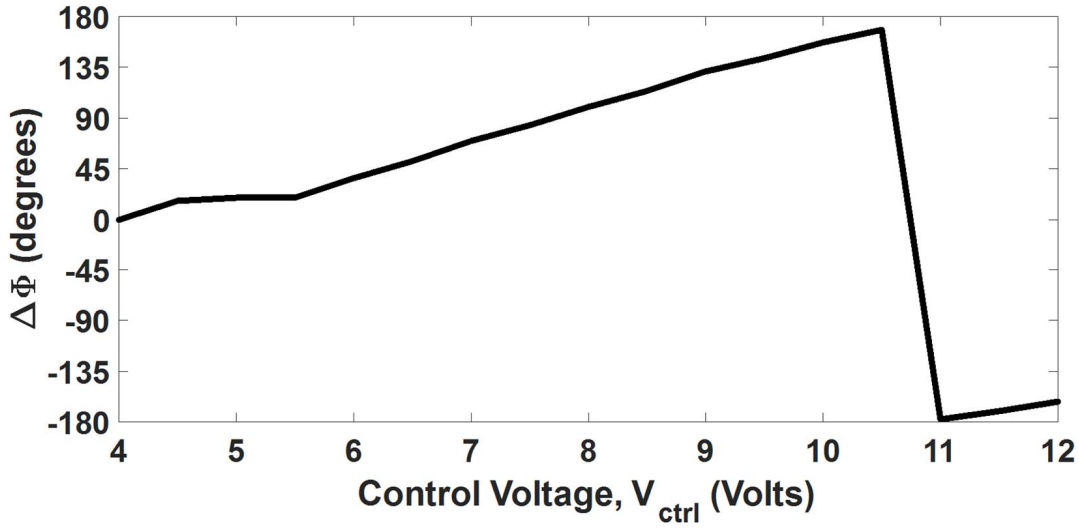

Figure 6.3. Measured normalized phase shifts introduced by the analog phase shifter for different control voltages (V_{ctrl}).

the required phase adjustments needed by the $\pm k^{\text{th}}$ element ($\Delta\phi^{\circ}_{\pm k}$) in the array are computed via the following equation:

$$\Delta\phi^{\circ}_{\pm k} = \frac{180}{\pi} \times \left(\frac{2\pi}{\lambda} \times \Delta z_{\pm k}\right) = \frac{180}{\pi} \times \left(\frac{2\pi}{\lambda} \times (z_m - z'_{\pm k})\right). \tag{6.6}$$

Finally, these computed phases are fed to the respective array elements using industrial standard analog phase shifters (Part No: HMC928LP5E) [37]. In Fig. 6, the measured normalized phase adjustment ($\Delta\phi^{\circ}$) offered by this phase shifter is plotted against a range of applied control voltages (V_{ctrl}). Although the changes in the x–coordinate values of array elements introduce some gain shifts due to the alteration of effective inter-element spacings, this limitation can be avoided to some extent by restricting the rotational movement of the array elements beyond certain threshold angles which altogether limit the flexibility of the array.

7. MEASUREMENTS AND RESULTS: VALIDATING S.M.A.R.T. PHASE CORRECTING TECHNIQUE

"*It doesn't matter how beautiful your theory is, it doesn't matter how smart you are. If it doesn't agree with experiment, it's wrong.*"

— Richard Feynman

7.1. Introduction

In this chapter, an implementation of the S.M.A.R.T. phase correction technique has been presented and validated using a comparison analysis between measurements, full-wave (HFSS [40]) simulation and analytical results. First, an algorithm was developed based on the novel S.M.A.R.T. phase correction technique. Then, an NI LabVIEW [38] Graphical User Interface (GUI) was designed to execute that algorithm in real-time and thus creating a self-adaptable system. Next, a 1×4 microstrip patch array was designed, prototyped and manufactured. Additionally, for ensuring proper conformal applications during measurements, the array was placed on four distinct setups of non-planar orientations with the help of custom built structures using additive manufacturing technology. Finally, for each conformal setup, measurements of the radiation patterns were performed and compared with simulations and analytical results for validating the proposed S.M.A.R.T. phase correction technique in conformal array antenna systems.

7.2. Implementation of S.M.A.R.T. Phase Correction Technique Using NI LabVIEW

Not only the proposed S.M.A.R.T. phase correction technique involves a fair amount of computations in real-time but also the analog sensor output voltage requires some trigonometric operations for extracting the information of the instantaneous inclination of the sensor. For that, a Graphical User Interface (GUI) in NI LabVIEW has been designed to perform all the above computations in real-time. Using two data acquisition interfaces, one NI-USB 6008 at sampling frequency 10kS/s and one NI-USB 6009 at 48 kS/s, as shown in Fig. 7.1, the GUI swiftly completes all the steps of the flowchart described in Fig. 7.2 in a serial manner. The last step of the flowchart is an additional stage where the GUI uses the evaluated coordinates of the array elements to display the instantaneous shape of the array using Bézier curves. This step acts as a runtime validation of

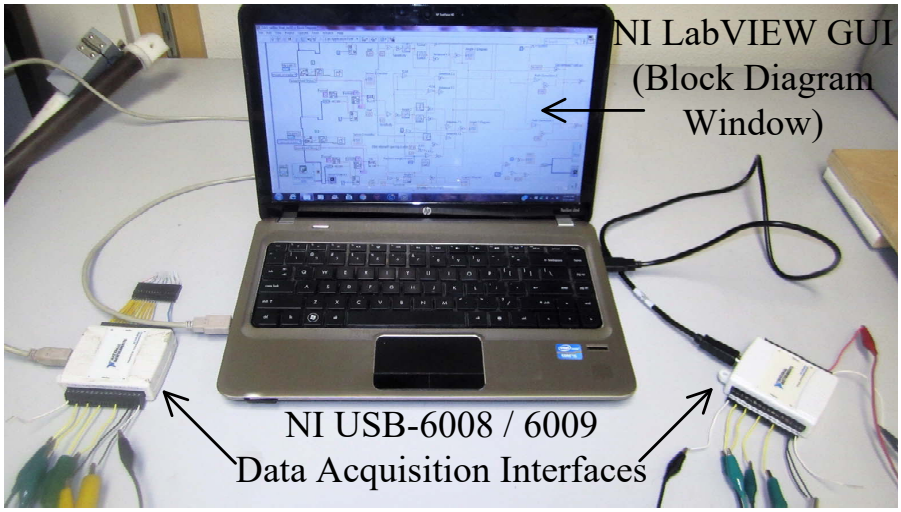

Figure 7.1. Benchtop setup of the NI LabVIEW GUI with two data acquisition interfaces for implementing S.M.A.R.T. phase correction technique in real-time using the developed algorithm.

the designed GUI and thus subsequently also validates the analytical S.M.A.R.T. phase correction method.

7.3. Prototyping the Conformal Array Antenna and S-Parameter Measurement

For measurement and demonstration purpose of the proposed theory, a 1×4 conformal array prototype using rectangular microstrip patch antennas on a Rogers RT/duroid 6006 [32] substrate with a dielectric thickness of 1.27 mm was investigated. These individual $50\ \Omega$ patches ($l = 24.5$ mm, $w = 32$ mm) resonate at 2.40 GHz ($d = \frac{\lambda}{2} = 62.5$ mm). Using a two-way, broadband, multi-channel power-splitter and four voltage controlled analog phase shifters, the feed and phase controlling network of the array were designed, respectively. The identical supporting platforms ($P_X = 62$ mm, $P_Y = 66$ mm, $P_Z = 25$ mm) were made of PolyActic Acid (PLA) and designed using additive manufacturing technology [39]. A complete setup of the antenna under test (A.U.T.) is shown in Fig. 7.3. All return losses measured at 2.40 GHz are recorded to be below 10 dB, as shown in Fig. 7.4, when the patches were connected to the phase shifter blocks, and a possible range of control voltages was applied to the phase shifters.

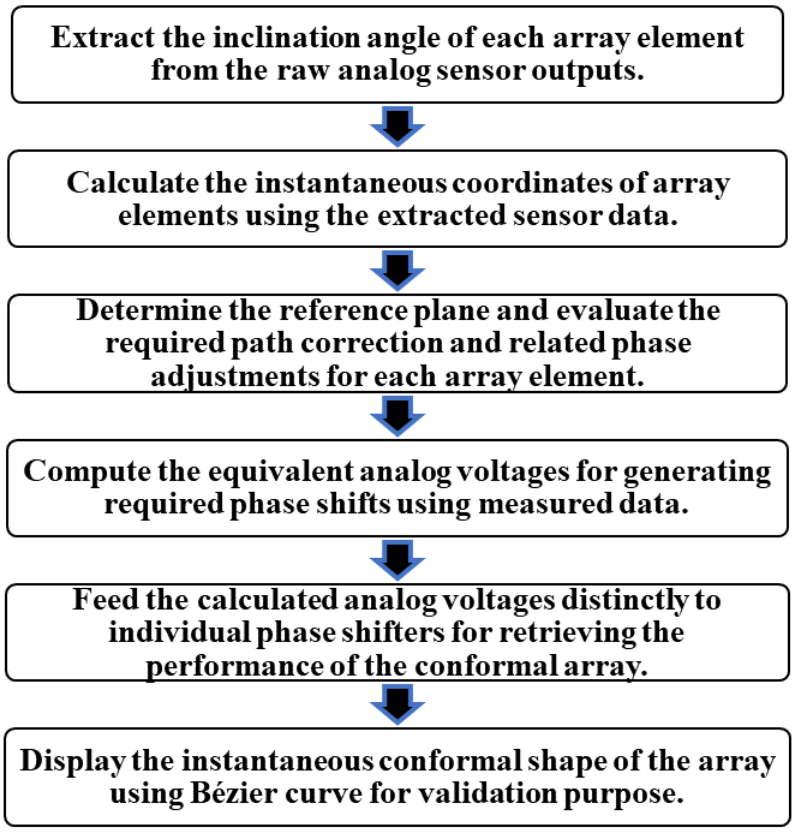

Figure 7.2. Flowchart followed by the NI LabVIEW GUI.

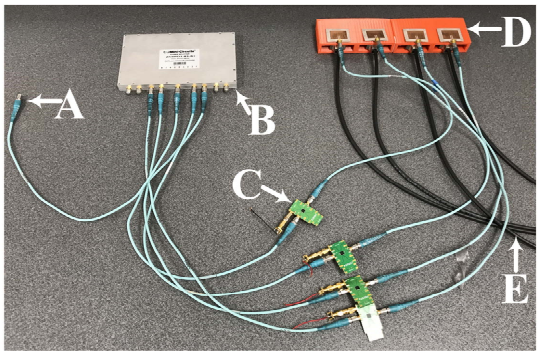

Figure 7.3. The integrated setup of the Antenna Under Test (A.U.T.).
Legends: A – Connection to the Vector Network Analyzer, B – Two-way power splitter, C – Voltage Controlled Analog Phase Shifters, D – Array Antenna with Supporting Platform, E – Inclinometer Connections to Labview GUI.

7.4. Pattern Correction Results

For measuring the radiation patterns of the A.U.T, an industrial standard TDK 1 GHz - 18 GHz horn antenna was used as the transmitter while the A.U.T. was treated as the receiver. The test setups in the anechoic chamber without and with the A.U.T are shown in Figs. 7.5 and 7.6, respectively. For validating the S.M.A.R.T. phase correction technique, four different non-planar orientations of the A.U.T. were considered. These conformal alignments consist of either two (Setup A, as shown in Fig. 7.7), three (Setup B, as shown in Fig. 7.9 and Setup C, as shown in Fig. 7.11) or four (Setup D, as shown in Fig. 7.13) different angles or points of curvature along the surface of the array. First, field patterns of each setup in the x–z plane were recorded without applying any external phase adjustment. These are termed here as the 'Uncorrected' patterns. Next, proper phase correction to the array elements in all four setups of the A.U.T. was applied via the LabVIEW GUI, followed by a repeated field pattern measurement in the x–z plane. These are termed here as the 'Corrected' patterns. The following equipments were used during the pattern measurements.

1. Transmitter: TDK 1 GHz - 18 GHz Horn Antenna (Model Number: HRN-0118);
2. Receiver: A.U.T;
3. Antenna Positioner: Model 6000 DC - 18 GHz Desktop Antenna Measurement System by Diamond Engineering (Step angle for azimuthal rotation: 1 degree); and
4. Network Analyzer and Data Recorder: Keysight E5071C 300 kHz - 20 GHz ENA Series Network Analyzer (Sweep setting: 1601 sweeps per degree, File format used for recording: *.csv*, Frequency: 2.40 GHz).

A comparison of the radiation patterns using analytical, HFSS simulations, and measurements for both uncorrected and corrected cases are shown in Figs. 7.8, 7.10, 7.12, and 7.14 for setups A, B, C, and D, respectively. Fair agreements were achieved for all the four cases. Moreover, the drops of $|\mathbf{E}_\theta|$ at $\theta = 0^\circ$ in all the uncorrected patterns have been recovered using the S.M.A.R.T. phase correction technique to achieve a maximum of $|\mathbf{E}_\theta|$ at $\theta = 0^\circ$ (hence, the maximum direction of radiation towards the broadside) in all the corrected patterns. Thus, it can be concluded now that the S.M.A.R.T. phase correction method has been succesfully validated.

7.5. Gain Calculation and Compensation Results

The gain of an antenna system to a particular direction can be defined by the total accepted power normalized by the corresponding isotropic intensity at that direction for the antenna. On the other hand, directivity of an antenna system towards a particular direction can be defined by the radiation intensity normalized by the corresponding isotropic intensity at that direction for the antenna. Theoretically if there is no loss due to the mutual coupling in the antenna system, the gain and the directivity will be the same. The mathematical relation between gain (G) and directivity (D) can be expressed as,

$$G = eD. \tag{7.1}$$

The term e in the equation (7.1) is known as the efficiency of the antenna system which may be defined as the ratio of the total power radiated by the antenna to the net power accepted by the antenna from the connected transmitter for an antenna system. Practically the gain of an antenna can never be equal to the directivity of that antenna as the gain depends also on the efficiency of the system. But to analyze the gain of a system, the analysis of directivity is required. So it can be said that if the efficiency of an antenna system does not change, the change in the directivity by a factor will lead to an equivalent change in the gain of the system by the same factor.

The above concept can be used also to analyze the gain of the array system described in this work. The directivity of an array can be found using the array factor (AF) equation [27],

$$D = \frac{4\pi |AF_{max}|^2}{\int_0^{2\pi}\int_0^{\pi} |AF|^2 \sin\theta \, \mathrm{d}\theta \mathrm{d}\phi}. \tag{7.2}$$

A uniform linear array of N number of elements with constant element spacing of d along the $z-$axis is symmetric with respect to ϕ and therefore the directivity of the array can be numerically computed and expressed as

$$D = \frac{N^2}{N + 2\sum_{n=1}^{N-1}(N-n)\,\mathrm{sinc}(nkd)\cos(nkd\cos\theta_s)}. \tag{7.3}$$

For the element spacing of $d = 0.5\lambda$, equation (7.3) simplifies to,

$$D \approx N. \tag{7.4}$$

For the element spacing up to a wavelength, the directivity increases almost in a linear fashion [29]. But as the element spacing increases further, the denominator in equation (7.3) also increases while the maximum value of AF in the numerator remains same. This results to a decrease in directivity of the array. Moreover, as the element spacing exceeds a wavelength, appearance of grating lobes results a sharp drop in directivity [27]. The decrease in directivity due to the grating lobe becomes more dramatic as the number of elements increases, because the main beam and grating lobes have narrower bandwidths which results in to a large change in AF for a small change in θ [29].

Refering to Fig. 5.3, when the surface of the array was bent in a certain angle, the phase shifter has been used to correct the radiation pattern. This has been done by adjusting the reference plane of the antenna. Although the array elements can be realized to be belonged virtually on a same plane by this phase compensation technique but a change in inter-element spacing can be noticed through this process. When the array element A_{+2} has been projected on the plane where A_{+1} was lying, the effective spacing between A_{+1} and projected A_{+2} got reduced by a factor of $(1 - \sin\theta_b)$. Now, as the default spacing was 0.5λ, therefore any further reduction of spacing would be result in a reduced directivity.

When the conformal array changes its shape, the associated gain of the overall array also changes. The reference gain $G_r(\theta, \phi)$ of the array can be defined as the gain of the array in a certain direction when the antenna array is attached to a flat surface. Now as the surface changes, the associated field pattern of the array also changes. Therefore, the uncompensated gain $G_U(\theta, \phi)$ ($<G_r(\theta, \phi)$, at broadside) of the array can then be defined as the new gain of the array before applying any phase correction in a certain direction when the array is attached on a conformal surface. When the phase correction method is applied to the array system, the shift in the gain of the antenna is observed. If this new compensated gain of the array system is denoted as $G_C(\theta, \phi)$ and the recovered gain of the array through the phase correction is described as $G_S(\theta, \phi)$ in simulations and $G_M(\theta, \phi)$ in measurements, then the following relationships hold true for all values of θ and ϕ:

$$G_S(\theta, \phi) = G_{C,simulation}(\theta, \phi) - G_{U,simulation}(\theta, \phi) \tag{7.5}$$

and

$$G_M(\theta, \phi) = G_{C,measured}(\theta, \phi) - G_{U,measured}(\theta, \phi). \tag{7.6}$$

The simulated and measured recovered gain values are shown in Fig. 7.15 for all four test cases (Setups A, B, C, and D). Although the radiation pattern can be recovered for an array antenna by S.M.A.R.T. phase correction technique but the trade-off will be thus a slight reduced gain resulting higher side lobe level and hence this is the limitation of the proposed technique.

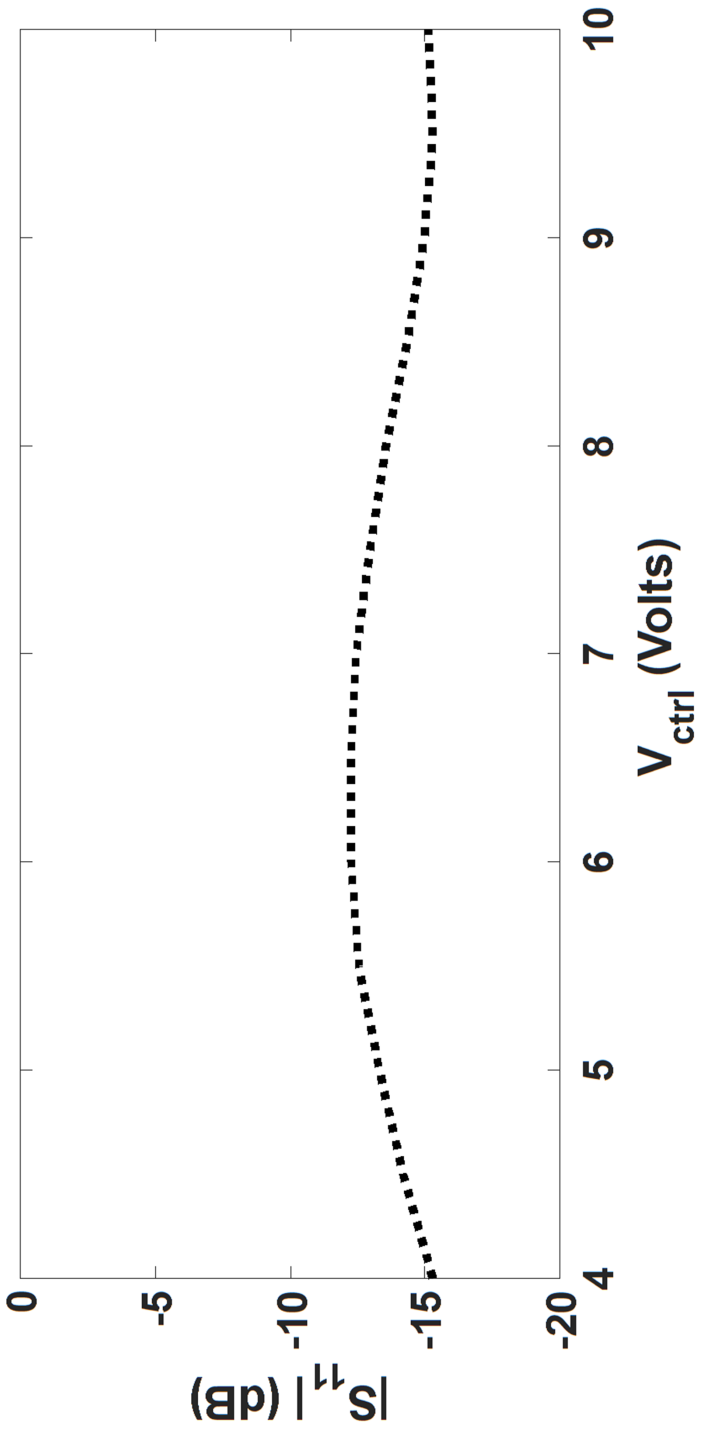

Figure 7.4. Return Loss of the A.U.T. while the phase shifter module was applied through different control voltages (V_{ctrl}).

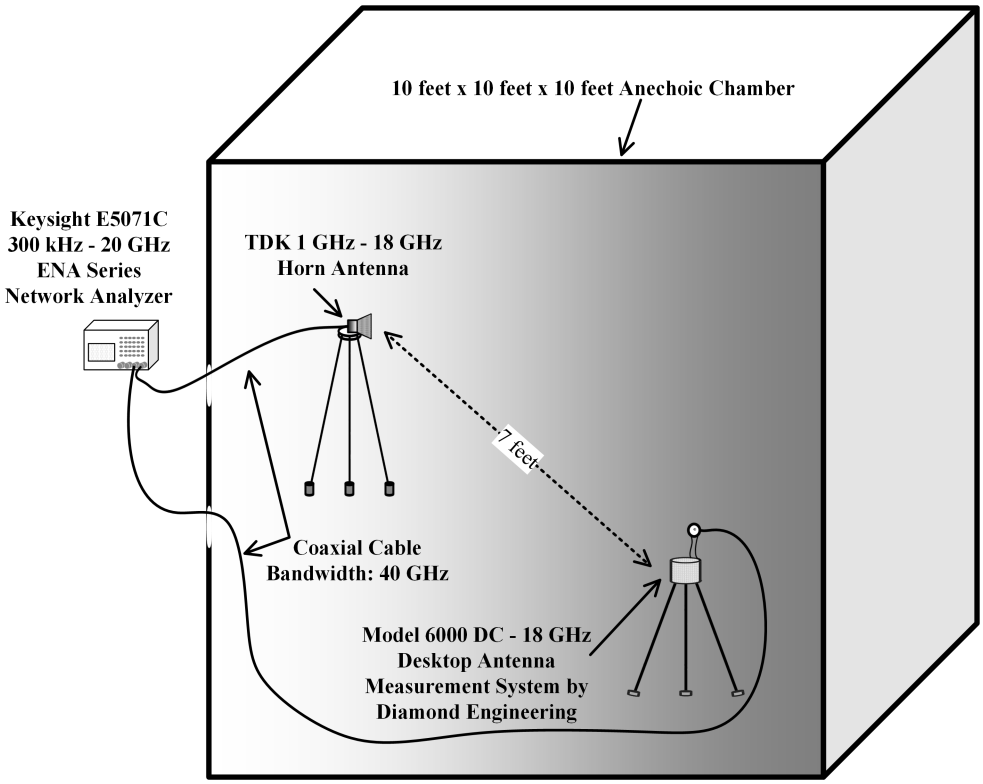

Figure 7.5. Test setup excluding A.U.T. during measurements in the anechoic chamber.

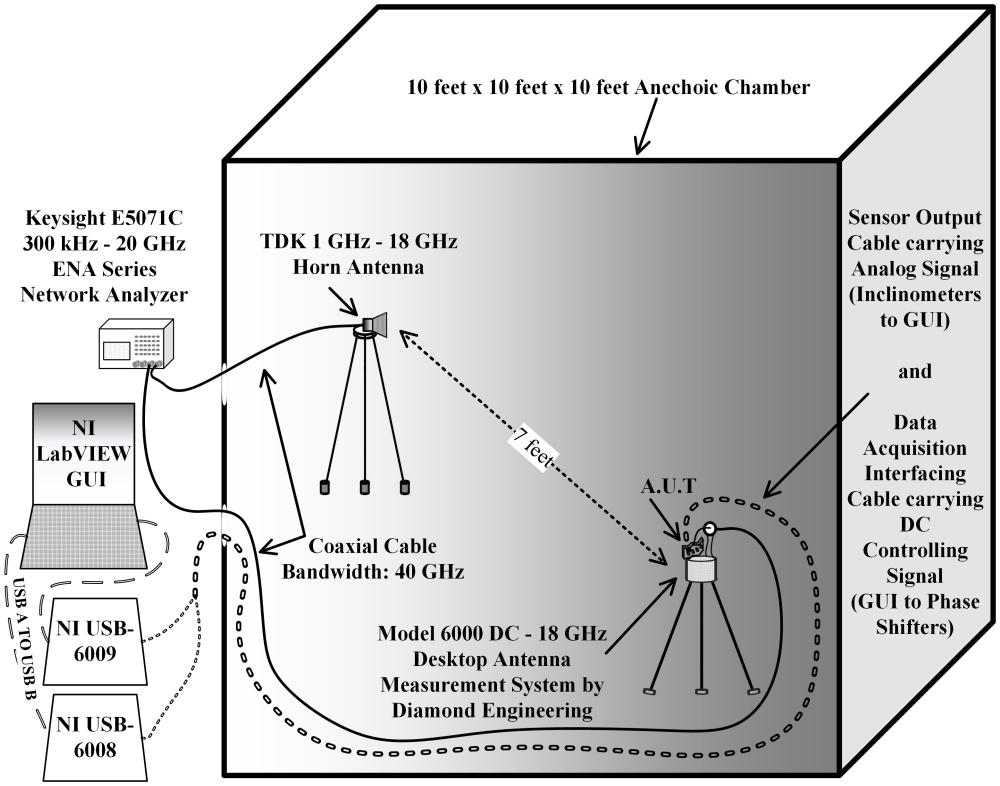

Figure 7.6. Test setup including A.U.T. during measurements in the anechoic chamber.

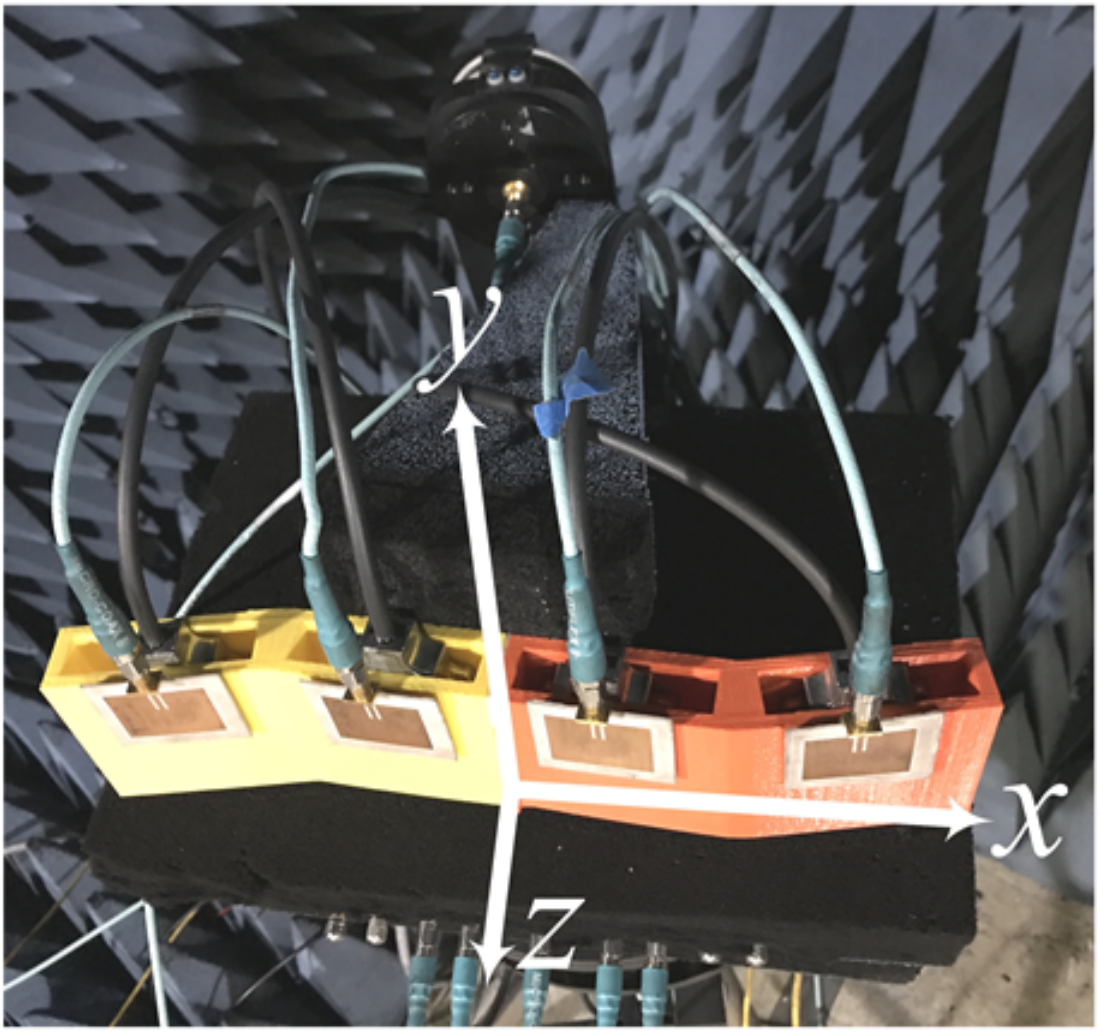

Figure 7.7. Image of Setup A during measurements in the anechoic chamber.

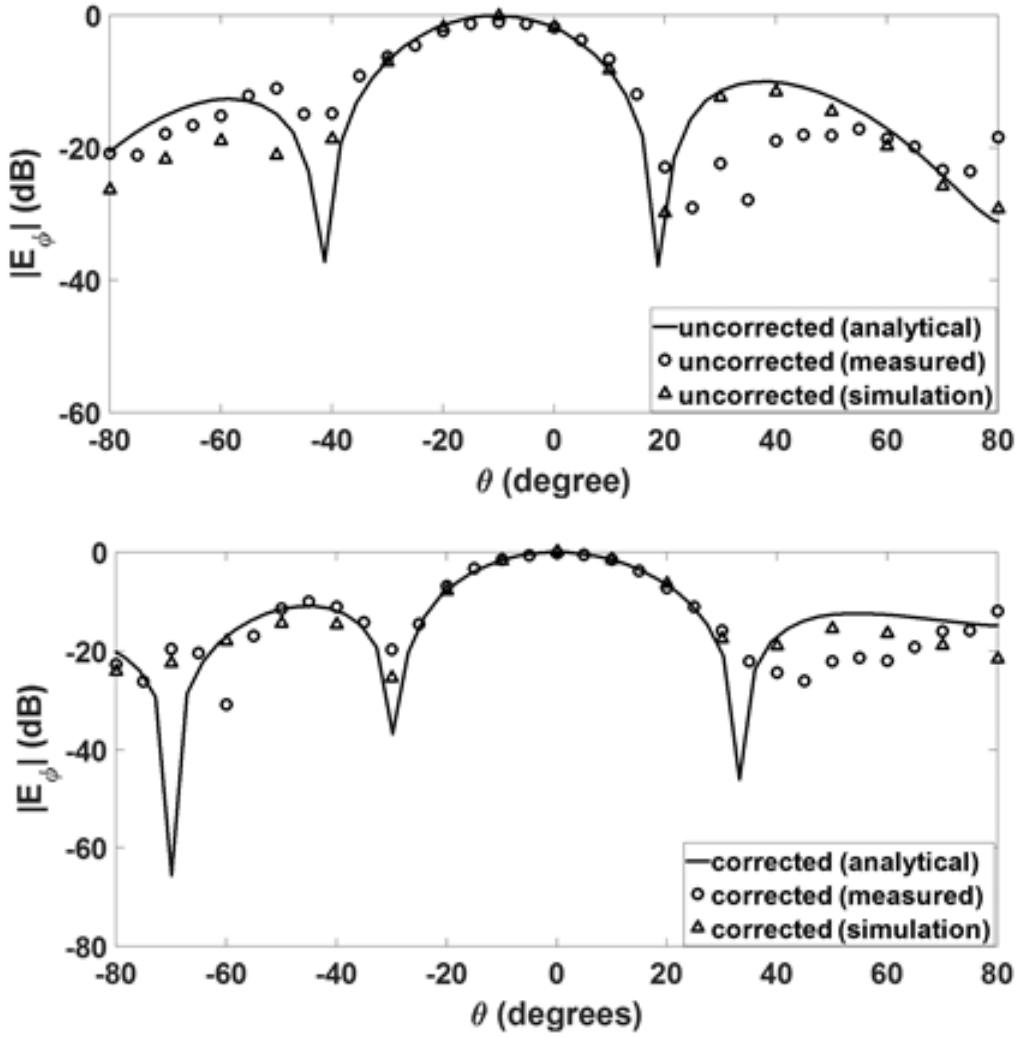

Figure 7.8. The uncorrected and corrected radiation patterns towards broadside at 2.40 GHz for Setup A.

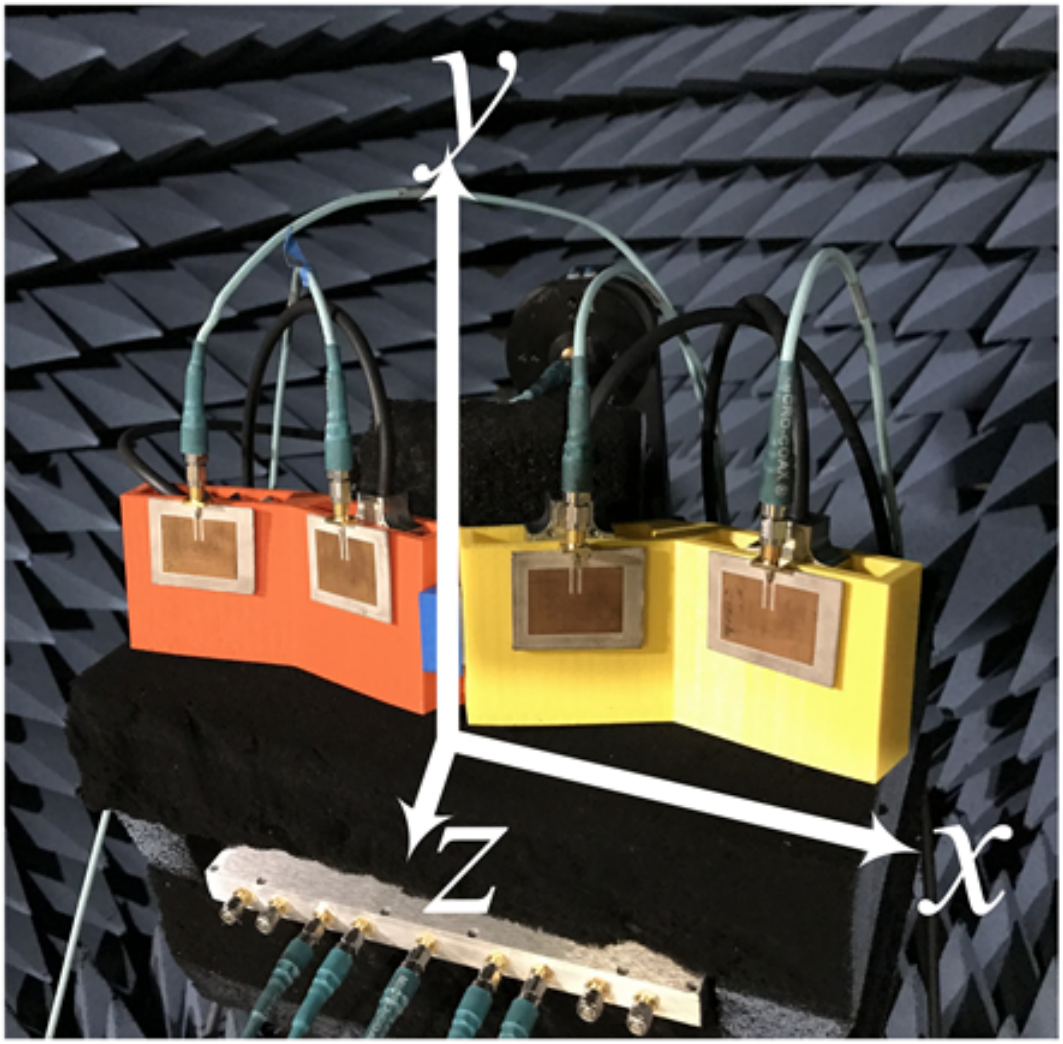

Figure 7.9. Image of Setup B during measurements in the anechoic chamber.

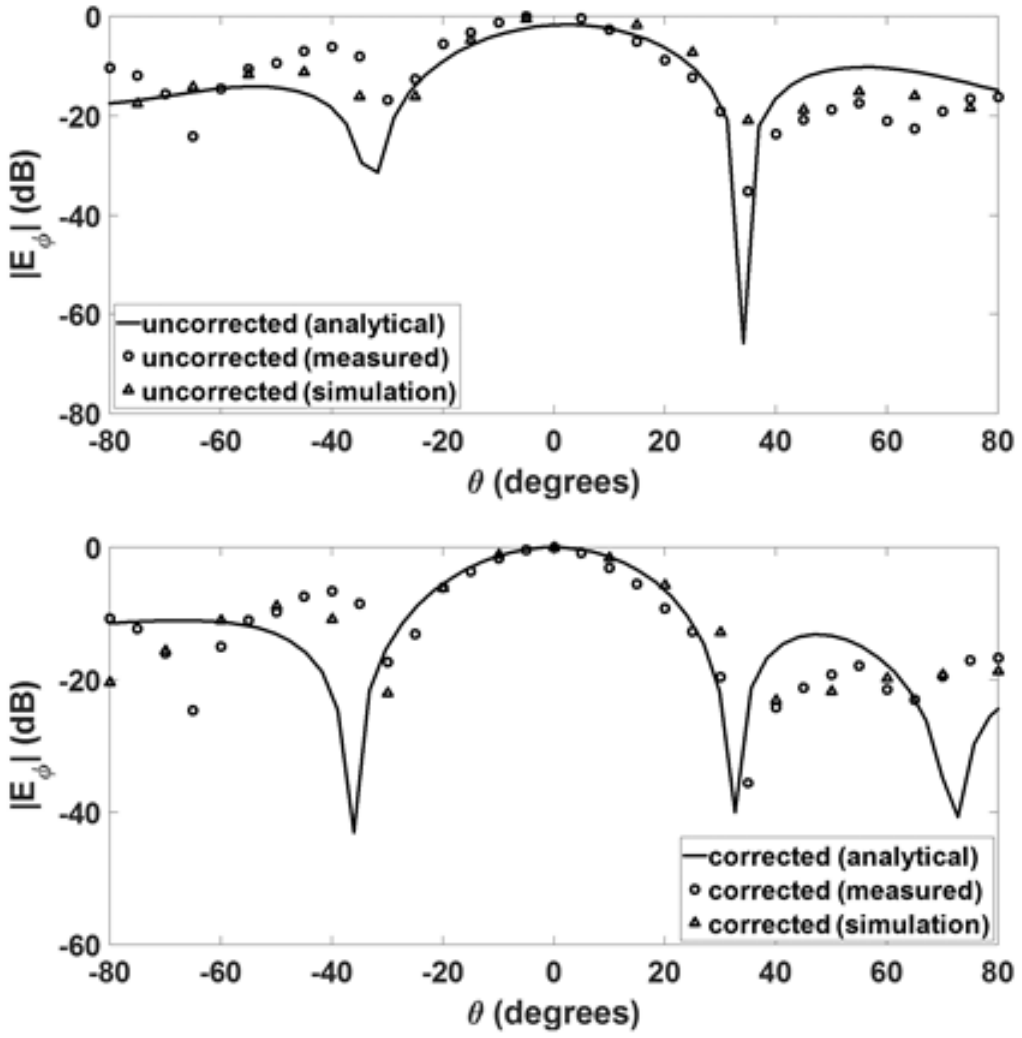

Figure 7.10. The uncorrected and corrected radiation patterns towards broadside at 2.40 GHz for Setup B.

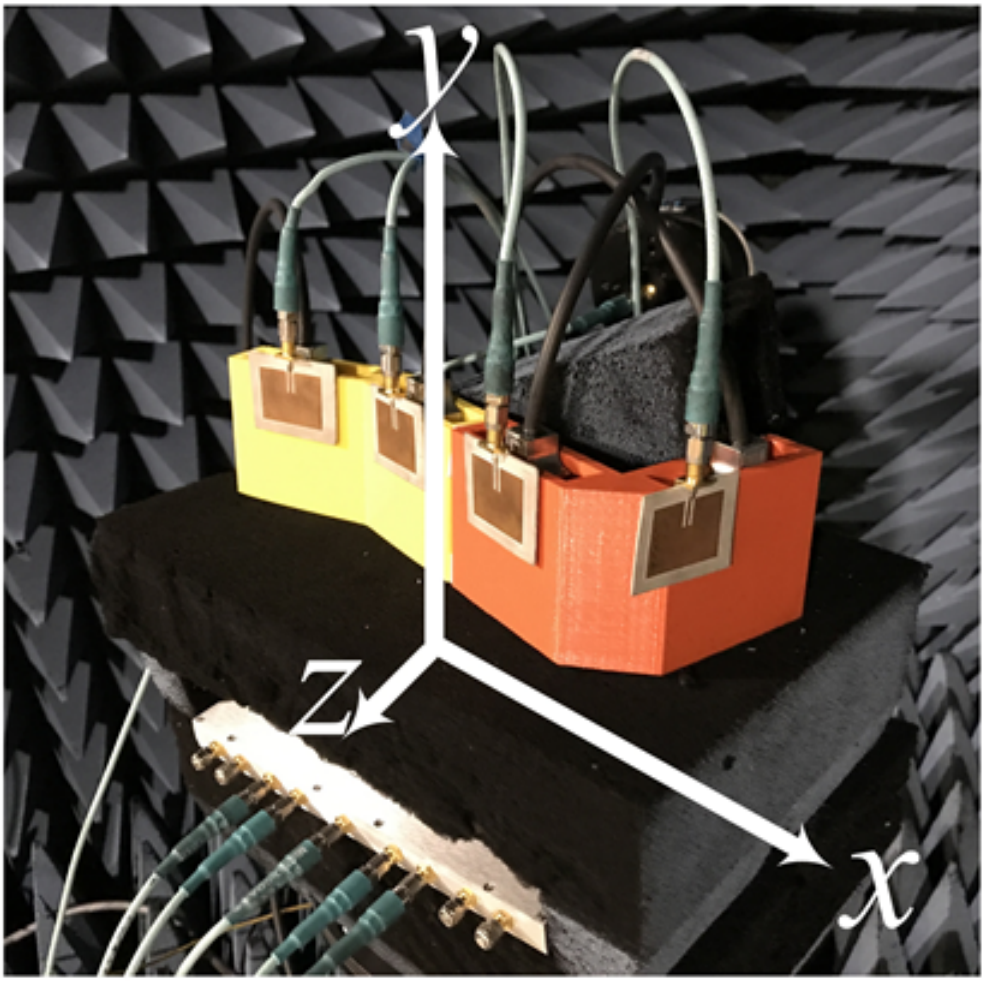

Figure 7.11. Image of Setup C during measurements in the anechoic chamber.

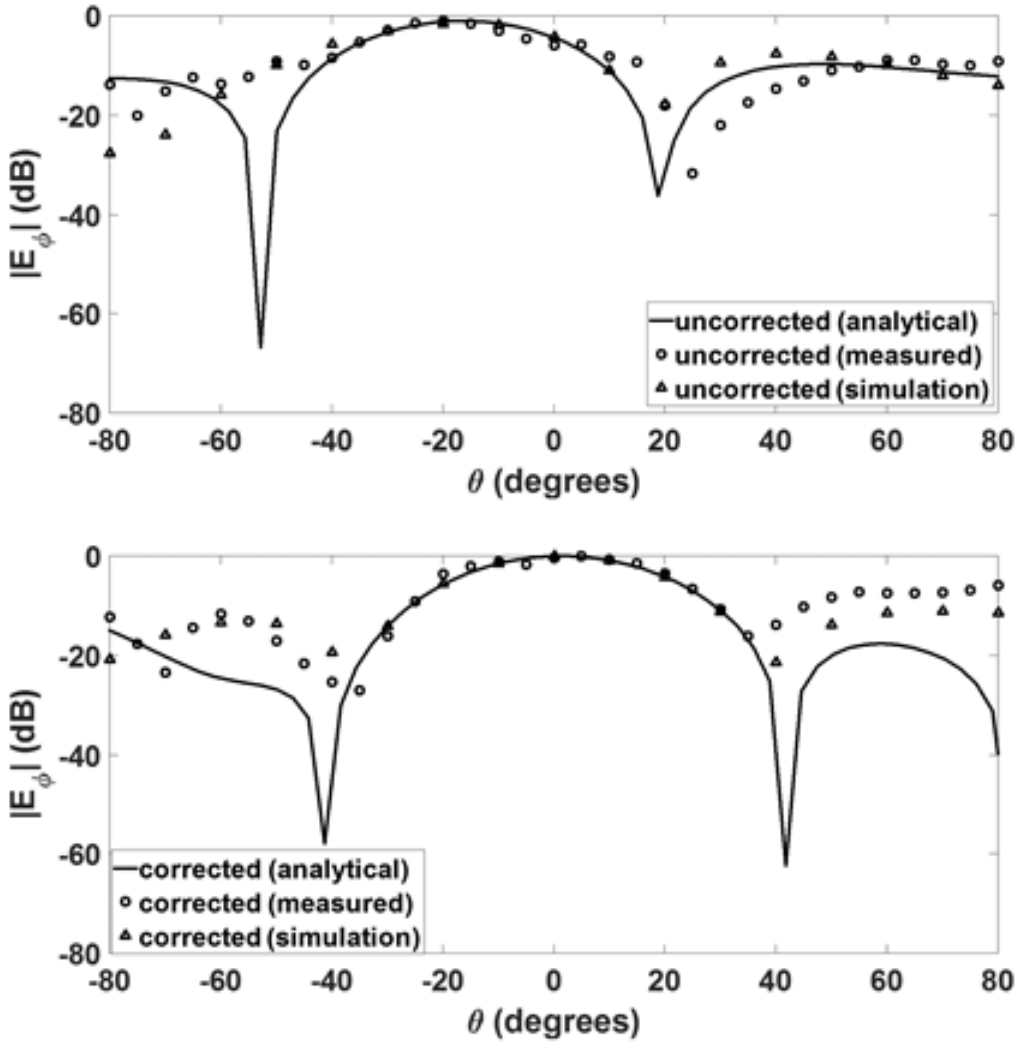

Figure 7.12. The uncorrected and corrected radiation patterns towards broadside at 2.40 GHz for Setup C.

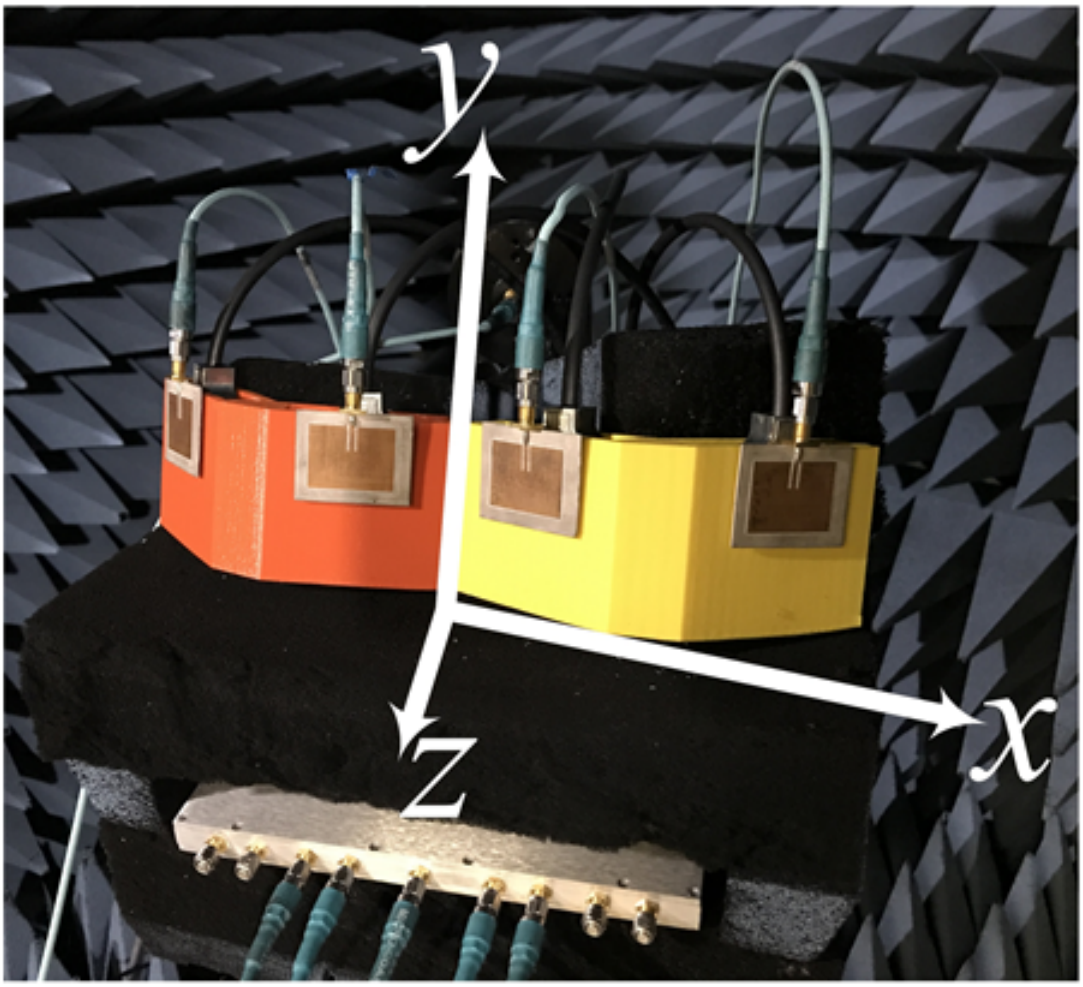

Figure 7.13. Image of Setup D during measurements in the anechoic chamber.

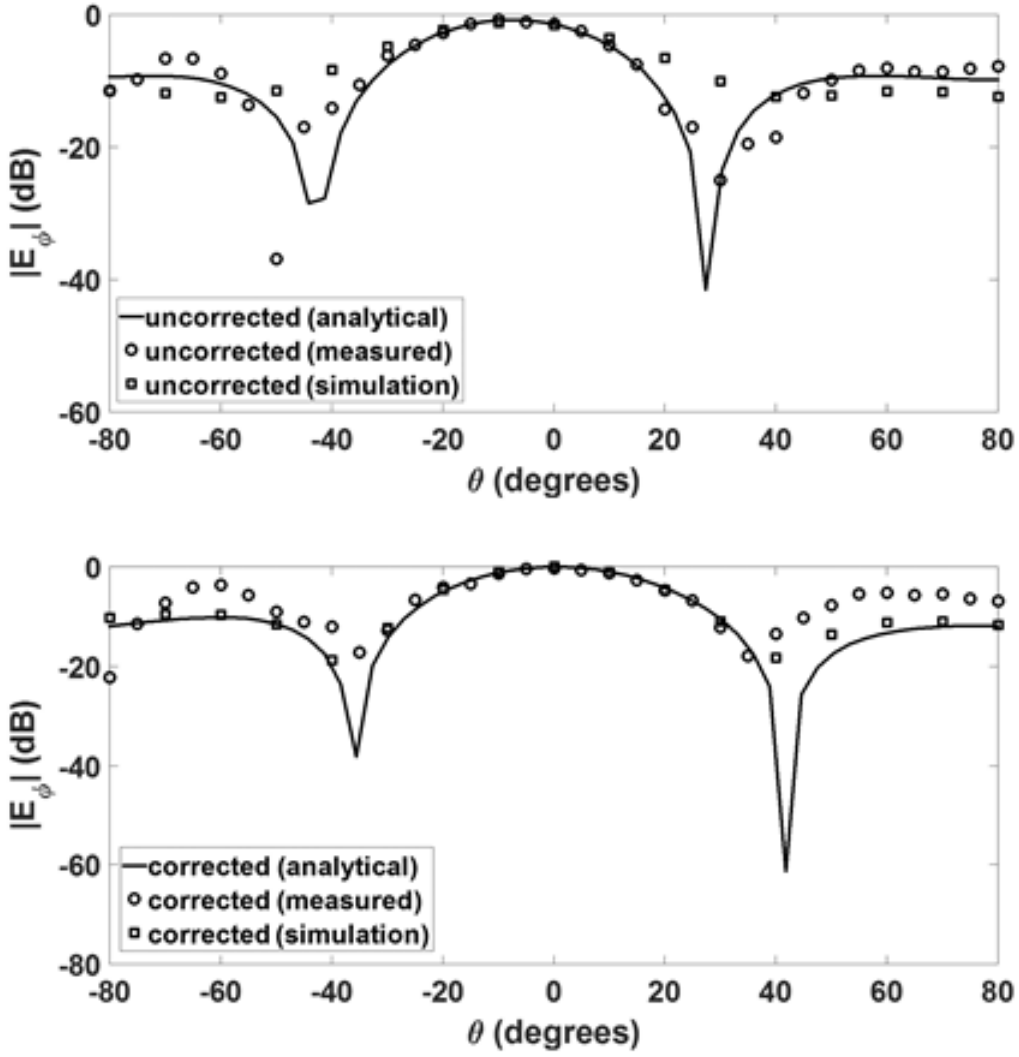

Figure 7.14. The uncorrected and corrected radiation patterns towards broadside at 2.40 GHz for Setup D.

Set	Angles of the array elements in the direction to the $\pm z$ axes with respective to the x–y plane: (degrees)				Index of the Reference Array Element:		Applied Phase-Corrections using S.M.A.R.T technique: (degrees)				Applied Control Voltage (V_{ctrl}) for the phase-shifter associated to the $\pm k^{th}$ element: (volts)					Simulated Recovered Gain, G_S: (dB)	Measured Recovered Gain, G_M: (dB)
	α_{-2}	α_{-1}	α_{+1}	α_{+2}	(m)	(k)	$\Delta\Phi_{-2}$	$\Delta\Phi_{-1}$	$\Delta\Phi_{+1}$	$\Delta\Phi_{+2}$	$k =$						
											-2	-1	+1	+2			
A	0	15	15	0	4	+2	92.4	69.3	23.1	0	6.8	6.1	4.6	3.9		3.9	3.2
B	0	30	-15	45	4	+2	106.2	61.6	40.1	0	7.2	5.8	5.2	3.9		2.6	2.4
C	0	30	30	-60	3	+1	133.9	89.3	0	32.7	8.0	6.7	3.9	4.9		5.7	4.4
D	60	-15	30	-45	3	+1	75.7	21.5	0	18.5	4.7	4.2	3.9	4.1		2.4	2.2

Figure 7.15. Test parameters for four different conformal antenna array setups including the recovered gain in both simulations and measurements achieved using S.M.A.R.T phase correction technique.

8. CONCLUSION

"*The true laboratory is the mind, where behind illusions we uncover the laws of truth.*"

— Jagadish Chandra Bose

A novel S.M.A.R.T. phase correction strategy for designing self-adapting conformal antenna arrays was presented in this dissertation. Using real-time spatial information of individual antenna elements, an inclinometer sensor determines the essential phase adjustment required by the respective array element. A LabVIEW GUI processes the sensor data and corrects the field pattern of the array in real-time. For validation, four different conformal setups were presented. Reasonable agreements between analytical, simulation and measurements are achieved both in the absence and in the presence of phase correction. Finally, during the experiments, a $2 - 4$ dB of shift in the antenna gain in both simulations and measurements was reported. Overall, the S.M.A.R.T. phase correction technique was proven to be very useful for realizing a self-adapting flexible array antenna on complex conformal surfaces and hence perfectly suitable for realizing next generation non-planar arrays. A summarized version of this dissertation has also been reported in [41].

REFERENCES

[1] R. M. Brian and R. S. Cohen (2007). Hans Christian Ørsted and the Romantic Legacy in Science, *Boston Studies in the Philosophy of Science,* Vol. 241.

[2] J. R. Hofmann, *André-Marie Ampère : Enlightenment and Electrodynamics,* Cambridge University Press, 2006.

[3] J. Hamilton, *A Life of Discovery: Michael Faraday, Giant of the Scientific Revolution,* Random House, 2004.

[4] J. C. Maxwell, *A treatise on electricity and magnetism Vol I,* Oxford: Clarendon Press, 1873.

[5] J. C. Maxwell, *A treatise on electricity and magnetism Vol II,* Oxford: Clarendon Press, 1873.

[6] T. K. Sarkar, R. Mailloux, A. A. Oliner, M. Salazar-Palma, D. L. Sengupta, *History of Wireless,* John Wiley and Sons, 2006.

[7] A. A. Huurdeman, *The Worldwide History of Telecommunications,* Wiley, 2003.

[8] V. Mukherji, *Jagadish Chandra Bose,* second edition, Builders of Modern India series, Publications Division, Ministry of Information and Broadcasting, Government of India, 1994.

[9] C. W. Bernard, *Tesla: Inventor of the Electrical Age,* Princeton University Press, 2013.

[10] S. Hong, *Wireless: From Marconi's Black-Box to the Audio,* Cambridge, Mass.: MIT Press, 2001.

[11] A. T. Story, *A Story of Wireless Telegraphy,* D. Appleton and company, 1904.

[12] C. A. Balanis, *Antenna Theory,* John Wiley and Sons, Ltd., Hoboken, New Jersey, 2005.

[13] L. Josefsson and P. Persson, *Conformal Array Antenna Theory and Design,* IEEE Antennas and Propagation Society, Sponsor, John Wiley and Sons, Ltd., Hoboken, New Jersey, 2006.

[14] D.Y. Khang, H. Jiang, Y. Huang and J. A. Rogers, "A Stretchable Form of Single-Crystal Silicon for High-Performance Electronics on Rubber Substrates," *Science*, vol. 311, no. 5758, Jan. 13th, pp. 208-212, 2006.

[15] Ahmadloo, M. and Mousavi, P., “A novel integrated dielectric-and conductive ink 3D printing technique for fabrication of microwave devices,” *2013 IEEE Int. Microwave Symposium*, pp. 1-3, June 2013.

[16] S. Moscato, R. Bahar, T. Le, M. Pasian, M. Bozzi, L. Perregrini and M. M. Tentzeris, “Infill-Dependent 3-D-Printed Material Based on NinjaFlex Filament for Antenna Applications, *IEEE Antennas and Wireless Propagation Letters*, vol. 15, pp. 1506-1509, 2016.

[17] Salonen, P., Kim J., and Rahmat-Samii Y., “Dual-band E-shaped patch wearable textile antenna,” *IEEE Antennas and Propagation Society International Symposium*, Vol. 1. pp. 466-469, 2005.

[18] H. Schippers, P. Knott, T. Deloues, P. Lacomme and M. R. Scherbarth, “Vibrating antennas and compensation techniques research in NATO/RTO/SET 087/RTG 50,” *IEEE Aerospace Conference*, Mar. 3-10, pp. 1-13, 2007.

[19] P.L. O’Donovan and A.W. Rudge, “Adaptive control of a flexible linear array,” *Electron. Lett.,* vol.9, no.6, pp.121-122, Mar. 22, 1973.

[20] B. D. Braaten, S. Roy, M. A. Aziz, S. Nariyal, I. Irfanullah, N. F. Chamberlain, M. T. Reich and D. E. Anagnostou, “A Self-Adapting Flexible (SELFLEX) Antenna Array for Changing Conformal Surface Applications,” *IEEE Trans. on Ant. and Prop.*, vol. 61, no. 2, Feb. pp. 655-665, 2013.

[21] B. D. Braaten, S. Roy, I. Irfanullah, S. Nariyal and D. E. Anagnostou, “Phase-Compensated Conformal Antennas for Changing Spherical Surfaces,” *IEEE Trans. on Ant. and Prop.*, vol. 62, no.4, pp. 1880–1887, 2014.

[22] S. Roy, “Designing of a Small Wearable Conformal Phased Array Antenna for Wireless Communications.” M.S. Thesis, North Dakota State University, 2012.

[23] B. Ijaz, A. Sanyal, A. Mendoza-Radal, S. Roy, I. Ullah, M. T. Reich, D. Dawn, B. D. Braaten, N. F. Chamberlain and D. E. Anagnostou,“Gain Limits of Phase Compensated Conformal Antenna Arrays on Non-Conducting Spherical Surfaces using the Projection Method,” *IEEE International Conference on Wireless for Space and Extreme Environments (WiSEE)*, Baltimore, MD, Nov. 7-9, 2013.

[24] I. Ullah, S. Nariyal, S. Roy, M. M. Masud, B. Ijaz, A. Aftikhar, S. A. Naqvi and B. D. Braaten, “A Note on the Fundamental Maximum Gain Limit of the Projection Method for Conformal Phased Array Antennas,” *Proceedings of the IEEE International Conference on Wireless Information Technology and Systems*, Maui, Hawaii, November 11th - 16th, 2012.

[25] F. T. Ulaby, *Fundamentals of Applied Electromagnetics,* Prentice Hall, New Jersey, 2001.

[26] S. Drabowitch, A. Papiernik, H. Griffith, J. Encinas and B. Smith, *Modern Antennas,* Chapman and Hall, London, 1998.

[27] R. C. Hansen, *Phased Array Antennas,* John Wiley and Sons, Inc., New York, NY, 1998.

[28] W. L. Stutzman and G. A. Thiele, *Antenna Theory and Design,* 2nd ed., John Wiley and Sons, Inc., New York, NY, 1998.

[29] R. L. Haupt, *Antenna Arrays: A Computational Approach,* John Wiley and Sons, Ltd., Hoboken, New Jersey, 2010.

[30] L. Piegl and W. Tiller, *The NURBS Book, 2nd ed.*, Springer-Verlag, NewYork, 1996.

[31] W. X. Jiang, J. Y. Chin, Z. Li, Q. Cheng, R. Liu, and T. J. Cui, “Analytical design of conformally invisible cloaks for arbitrarily shaped objects,” *Physical Review*, 066607, vol. E 77, no. 6, 2008.

[32] Rogers Corporation, [online] www.rogerscorp.com.

[33] A. Riškus, “Approximation of a cubic Bézier curve by circular arcs and vice versa,” *Info. Techno. and Control,* vol. 35, no. 4, pp. 371-378, 2006.

[34] S. Roy, B. Ijaz and B. D. Braaten,“Using Bézier Curves to Design Self-Adapting Conformal Phased-Array Antennas,” *Proceedings of the 2014 IEEE International Symposium on Antennas and Propagation,* Jul. 6 - 12, 2014, Memphis, TN, pp. 1786 - 1787.

[35] B. D. Braaten, M. A. Aziz, S. Roy, S. Nariyal, N. F. Chamberlain and D. E. Anagnostou,“Half-Power Beamwidth of a Self-Adapting Conformal 1 x 4 Microstrip Array,” *Proceedings of the 2012 IEEE International Symposium on Antennas and Propagation*, Chicago, IL, July 2012.

[36] Murata Manufacturing, [online] http://www.murata.com.

[37] Hittite Microwave Corporation, [online] www.analog.com.

[38] National Instruments Corporation, [online] www.ni.com.

[39] Makerbot, [online] www.makerbot.com

[40] Ansys Inc., Ansys HFSS, Version 13.0.1, [online] www.ansys.com

[41] S. Roy, S. Sajal and BD. Braaten, “A phase correction technique based on spatial movements of antennas in real-time for designing self-adapting conformal array antennas.” *Microw Opt Technol Lett.* 2017;59:3002-3010.